GEOMETRY-CONFORMING FINITE ELEMENT METHODS FOR INTERFACE PROBLEMS ON FITTED AND UNFITTED MESHES

YUANHUI LIN, TAO LIN, XU ZHANG, AND MINFU FENG

ABSTRACT. We develop an arbitrary-degree geometry-conforming finite element (GC-FE) framework for two-dimensional elliptic boundary value and interface problems on curved domains. Using the Frenet–Serret transformation, curved-boundary and interface-fitted segments are represented exactly, while polynomials in Frenet coordinates generate generally nonpolynomial local shape functions in physical coordinates. For interface-unfitted meshes, GC-FE spaces on curved-boundary elements are coupled with geometry-conforming immersed finite element (GC-IFE) spaces on interface-cut elements, with standard polynomial spaces used elsewhere. We establish optimal approximation, inverse, and trace estimates for the GC-FE spaces. For fitted meshes, we prove well-posedness and optimal error estimates in energy and L^2 norms for a symmetric interior penalty discontinuous Galerkin discretization. By retaining the prescribed curves exactly, the method avoids the geometric variational crime associated with curved-geometry approximation and requires no corresponding geometric consistency estimates. Numerical experiments confirm the predicted rates, show global accuracy comparable to nodal isoparametric finite elements and smaller true-interface trace errors in the reported tests, and demonstrate the coupled GC-FE-GC-IFE method on interface-unfitted meshes.

1. INTRODUCTION

Let $\Omega \subset \mathbb{R}^2$ be a bounded domain with smooth boundary $\partial\Omega$, and consider the second-order elliptic boundary value problem

$$-\nabla \cdot (\beta \nabla u) = f \quad \text{in } \Omega, \tag{1.1}$$

$$u = g \quad \text{on } \partial\Omega. \tag{1.2}$$

We also consider the closely related *elliptic interface problem*. Let Γ_i be a smooth curve that divides Ω into two subdomains Ω^+ and Ω^-, and let β be uniformly positive and piecewise smooth, with a possible jump across Γ_i. We seek u satisfying

$$-\nabla \cdot (\beta \nabla u) = f \quad \text{in } \Omega^+ \cup \Omega^-, \tag{1.3}$$

$$u = g \quad \text{on } \partial\Omega, \tag{1.4}$$

together with the interface jump conditions

$$[\![u]\!]_{\Gamma_i} = 0, \qquad [\![\beta \partial_{\mathbf{n}} u]\!]_{\Gamma_i} = 0, \tag{1.5}$$

where $\mathbf{n}$ is a unit normal to Γ_i and $[\![\cdot]\!]_{\Gamma_i}$ denotes the jump across the interface. Boundary value problems of the form (1.1)–(1.2) and interface problems of the form (1.3)–(1.5) arise widely in science and engineering, including heat conduction, porous-media flow, electromagnetics, and the modeling of composite and multiphase materials. In these applications, the curved boundary $\partial\Omega$ or interface Γ_i carries essential physical and geometric information.

Both problems present a common geometric difficulty. When a curved domain is approximated by a straight-edged mesh, the polygonal boundary generally differs from the physical boundary by $O(h^2)$. For high-order finite element spaces, the resulting geometric consistency error may dominate the discretization error unless the geometry is approximated to a correspondingly high order. Such a domain perturbation is a classical example of a *variational crime* in the sense of Strang [12, 32]. An analogous issue arises in interface problems, where the jump conditions (1.5) should ideally be imposed on the physical interface Γ_i rather than on a polygonal approximation. Accurate treatment of curved boundaries and interfaces is therefore essential for the analysis and implementation of high-order finite element methods.

A classical remedy is the isoparametric finite element method. In this approach, a curved computational element K_h is defined as the image $K_h = F_K(\widehat{K})$ of a reference simplex $\widehat{K}$ under a polynomial mapping $F_K \in [\mathbb{P}_m(\widehat{K})]^2$. The degree of the geometric mapping is typically matched to that of the corresponding finite element space. Detailed treatments can be found in [12, 32], and the isoparametric framework has also been extended to high-order discretizations of elliptic interface problems [24].

The isoparametric approach is well established and supported by a comprehensive approximation theory. In its standard form, however, a general curved geometry is represented by piecewise polynomial mappings. Unless the physical geometry lies in the chosen polynomial mapping space, the computational geometry remains an approximation. Moreover, constructing a valid high-order curved mesh can be nontrivial, particularly when the curvature is large relative to the local mesh size, because the element mappings must remain regular and the curved elements remain non-inverted. Although suitably constructed isoparametric elements retain optimal approximation orders, their analysis must quantify the discrepancy between the physical and computational geometries and the resulting perturbations of the variational formulation [10, 11, 23]. Controlling these geometric consistency errors thus introduces an additional issue beyond standard finite element approximation analysis.

For interface problems, the geometric challenge is at least as significant. An interface-fitted mesh must conform either to the physical interface or to a sufficiently accurate approximation, and changes in the interface geometry may require costly remeshing. Immersed finite element (IFE) methods alleviate these difficulties by using meshes independent of the interface and modifying the local finite element functions on interface elements to incorporate the jump conditions (1.5), while retaining standard polynomial spaces on non-interface elements. Following their introduction and early development [19, 25, 26], IFE methods have been studied extensively. Subsequent developments include partially penalized formulations with optimal-order error estimates [27], higher-degree constructions based on least-squares procedures [3] and Cauchy extensions [15], three-dimensional a priori analyses [16, 18], and extensions to other classes of partial differential equations [7–9, 17, 20, 28].

More recently, the *Frenet–Serret apparatus* from differential geometry has been used to represent curved interfaces exactly while retaining high-order approximation. A tubular neighborhood of the interface is mapped to a coordinate strip in which the interface is straightened. The jump conditions can then be imposed on the exact interface, and geometry-conforming immersed finite element (GC-IFE) spaces of arbitrary polynomial degree can be constructed systematically [4, 5]. This construction incorporates the tangent and normal fields, together with the interface curvature, directly into the local approximation space. It has recently been extended from Cartesian meshes to unstructured triangular meshes [29].

The central observation of this paper is that the Frenet–Serret transformation (hereafter, Frenet transformation) is not limited to immersed finite element discretizations; it also provides an intrinsic, geometry-conforming alternative to isoparametric mappings for curved boundaries and fitted interfaces. Based on this observation, we develop and analyze a *geometry-conforming finite element (GC-FE)* method for two-dimensional elliptic boundary value and interface problems. On each curved-boundary or interface-fitted element, the exact physical curve forms an element edge — a geometry-exact construction that introduces no surrogate geometry — while polynomials in Frenet coordinates generate generally nonpolynomial shape functions in physical coordinates. On interface-unfitted meshes, the GC-FE spaces are combined with the GC-IFE spaces of [29], which impose the interface jump conditions on the exact interface within each cut element. Consequently, the computational domain coincides exactly with Ω for curved-boundary problems, and both fitted and unfitted discretizations retain the exact physical interface. This geometric conformity eliminates the separate domain- and interface-perturbation terms that arise in classical isoparametric analysis [10, 11, 23].

The principal contributions of this paper are summarized as follows.

(i) **Geometry-conforming finite element spaces of arbitrary degree.** We introduce a systematic construction of arbitrary-degree finite element spaces on elements adjacent to curved boundaries and fitted interfaces. The construction retains the exact physical curve as an element edge and, unlike the classical isoparametric approach, requires no polynomial surrogate for the curved geometry.

(ii) **A unified treatment of fitted and unfitted meshes.** GC-FE spaces are used on fitted elements with curved interface edges, whereas GC-IFE spaces [29] are used on interface-cut elements of unfitted triangular meshes, with standard polynomial spaces retained elsewhere. In both settings, the corresponding geometry-conforming spaces treat the physical interface exactly.

(iii) **Crucial estimates for the resulting nonpolynomial spaces.** We establish optimal-order approximation properties for the GC-FE spaces, showing that the transformation to nonpolynomial functions in physical coordinates preserves the approximation capability of the underlying polynomial spaces in Frenet coordinates. Additionally, we prove inverse and trace inequalities for the GC-FE spaces.

(iv) **Optimally convergent discontinuous Galerkin discretizations based on GC-FE spaces.** We formulate symmetric interior penalty discontinuous Galerkin (SIPDG) methods for the boundary value problem (1.1)–(1.2) and the interface problem (1.3)–(1.5). Because the physical boundary and interface are retained exactly, the analysis requires no separate consistency estimates associated with geometric approximation.

The remainder of the paper is organized as follows. Section 2 recalls the Frenet–Serret transformation and establishes the necessary geometric preliminaries. Section 3 constructs the GC-FE space and derives its approximation properties, inverse inequalities, and trace inequalities. Section 4 develops the SIPDG discretization, proves its well-posedness and optimal a priori error estimates in the energy and L^2 norms, and shows how exact geometric conformity eliminates the need for a separate geometric-consistency estimate. Section 5 presents numerical experiments, including a comparison with the isoparametric method and a test of the combined GC-FE-GC-IFE discretization on an interface-unfitted mesh. Section 6 concludes the paper.

2. Preliminaries

In this section, we recall the Frenet transformation and establish the geometric estimates used in the construction and analysis of the GC-FE spaces. Some of these results have appeared previously in [4–6]; they are included here for completeness.

2.1. **Geometric setting and mesh classification.** Let $\Omega \subset \mathbb{R}^2$ be a bounded domain with a smooth boundary Γ_b. Let $\Gamma_i \subset \Omega$ be a smooth curve that separates Ω into two disjoint open subdomains Ω^- and Ω^+ such that

$$\Omega = \Omega^- \cup \Gamma_i \cup \Omega^+.$$

For $t = b, i$, we assume that Γ_t admits a regular C^2 parameterization

$$\mathbf{g}_t(\xi) = \begin{bmatrix} g_{t1}(\xi) \\ g_{t2}(\xi) \end{bmatrix}, \qquad \xi \in [\xi_s, \xi_e]. \tag{2.1}$$

Let $\{\overline{\mathcal{T}}_h\}_{h>0}$ be a family of shape-regular, straight-sided precursor triangulations associated with Ω. We say that an edge of an element $\overline{K} \in \overline{\mathcal{T}}_h$ fits a curve if both endpoints of the edge lie on the curve. We define

$$\overline{\mathcal{T}}_h^i := \{\overline{K} \in \overline{\mathcal{T}}_h : \overline{K} \text{ is cut by } \Gamma_i \text{ and has no edge fitted to } \Gamma_i\},$$
$$\overline{\mathcal{T}}_h^c := \{\overline{K} \in \overline{\mathcal{T}}_h : \overline{K} \text{ has a designated edge fitted to } \Gamma_b \text{ or } \Gamma_i\}.$$

We assume, without loss of generality, that $\overline{\mathcal{T}}_h^i \cap \overline{\mathcal{T}}_h^c = \varnothing$ and define

$$\overline{\mathcal{T}}_h^r := \overline{\mathcal{T}}_h \setminus \left(\overline{\mathcal{T}}_h^i \cup \overline{\mathcal{T}}_h^c\right).$$

Thus, every element of $\overline{\mathcal{T}}_h$ belongs to exactly one of the three classes.

The elements of $\overline{\mathcal{T}}_h^i$ are called *interface elements*, whereas those of $\overline{\mathcal{T}}_h^c$ are called *precursor curved elements*. The elements in $\overline{\mathcal{T}}_h^r$ are called *regular elements*. We say that the mesh $\overline{\mathcal{T}}_h$ is *interface-fitted* if $\overline{\mathcal{T}}_h^i = \varnothing$ and *interface-unfitted* otherwise. Examples of interface-fitted and interface-unfitted meshes are shown in Figure 1.

For each $\overline{K} \in \overline{\mathcal{T}}_h^c$, let $K = K(\overline{K})$ be the curved triangle obtained by replacing its designated straight edge with the corresponding arc of Γ_b or Γ_i. We then set

$$\mathcal{T}_h^i := \overline{\mathcal{T}}_h^i, \qquad \mathcal{T}_h^c := \{K(\overline{K}) : \overline{K} \in \overline{\mathcal{T}}_h^c\}, \qquad \mathcal{T}_h^r := \overline{\mathcal{T}}_h^r,$$

and define the resulting curved mesh of Ω by

$$\mathcal{T}_h := \mathcal{T}_h^i \cup \mathcal{T}_h^c \cup \mathcal{T}_h^r.$$

We assume that the curved mesh family $\{\mathcal{T}_h\}_{h>0}$ is shape-regular in the following sense. For each $K \in \mathcal{T}_h$, let $h_K := \mathrm{diam}(K)$ and define its inradius by

$$\rho_K := \sup\{r > 0 : \text{there exists } X \in K \text{ such that } B(X, r) \subset K\}. \tag{2.2}$$

We assume that there exists a constant $C_{\text{sh}} > 0$, independent of h and K, such that

$$\frac{h_K}{\rho_K} \le C_{\text{sh}}, \qquad \forall\ h > 0, \quad K \in \mathscr{T}_h. \tag{2.3}$$

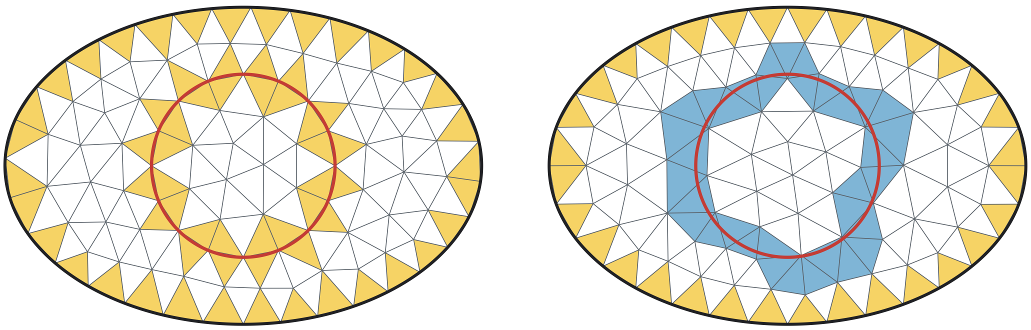

FIGURE 1. An elliptical domain with a circular interface. Left: an interface-fitted mesh; right: an interface-unfitted mesh. Regular elements ($\overline{\mathscr{T}}_h^r$), precursor curved elements ($\overline{\mathscr{T}}_h^c$), and interface elements ($\overline{\mathscr{T}}_h^i$) are shown in white, gold, and blue, respectively. The gray edges outline the precursor triangulations, the thick dark curve represents the outer boundary Γ_b, and the red circle represents the interface Γ_i.

2.2. **Frenet coordinates and uniform map estimates.** Consider a regular C^2 curve $\Gamma \subset \mathbb{R}^2$ parameterized by

$$\mathbf{g}(\xi) = \begin{bmatrix} g_1(\xi) \\ g_2(\xi) \end{bmatrix}, \qquad \xi \in [\xi_s, \xi_e]. \tag{2.4}$$

The Frenet–Serret apparatus [2, 30] associated with the curve $\mathbf{g}(\xi)$ consists of the unit tangent $\boldsymbol{\tau}(\xi)$, the unit normal $\mathbf{n}(\xi)$, and the curvature $\kappa(\xi)$:

$$\boldsymbol{\tau}(\xi) = \frac{\mathbf{g}'(\xi)}{\|\mathbf{g}'(\xi)\|}, \qquad \mathbf{n}(\xi) = Q\boldsymbol{\tau}(\xi), \qquad \kappa(\xi) = \frac{\mathbf{g}'(\xi)^T Q \mathbf{g}''(\xi)}{\|\mathbf{g}'(\xi)\|^3}, \tag{2.5}$$

where

$$Q = \begin{bmatrix} 0 & 1 \\ -1 & 0 \end{bmatrix}.$$

The associated Frenet transformation $P_\Gamma : (\eta, \xi) \to (x, y)$ is

$$\mathbf{x}(\eta, \xi) = \begin{bmatrix} x(\eta, \xi) \\ y(\eta, \xi) \end{bmatrix} = P_\Gamma(\eta, \xi) := \mathbf{g}(\xi) + \eta \mathbf{n}(\xi). \tag{2.6}$$

The tubular-neighborhood theorem [1] implies that Γ has an ϵ-tubular neighborhood

$$N_\Gamma(\epsilon) := P_\Gamma\big([-\epsilon, \epsilon] \times [\xi_s, \xi_e]\big)$$

on which the transformation P_Γ is a bijection. Its inverse is denoted by

$$\begin{aligned} R_\Gamma = P_\Gamma^{-1} : N_\Gamma(\epsilon) &\longrightarrow [-\epsilon,\epsilon]\times[\xi_s,\xi_e], \\ \begin{bmatrix}\eta\\ \xi\end{bmatrix} &= R_\Gamma(x,y) = \begin{bmatrix}\eta(x,y)\\ \xi(x,y)\end{bmatrix}. \end{aligned} \tag{2.7}$$

A direct calculation gives

$$\nabla\eta(x,y) = \mathbf{n}(\xi), \tag{2.8}$$

$$\nabla\xi(x,y) = \left\|\mathbf{g}'(\xi)\right\|^{-1}\left(1+\eta\kappa(\xi)\right)^{-1}\boldsymbol{\tau}(\xi), \tag{2.9}$$

$$DP_\Gamma(\eta,\xi) = \left[\mathbf{n}(\xi), \left\|\mathbf{g}'(\xi)\right\|\left(1+\eta\kappa(\xi)\right)\boldsymbol{\tau}(\xi)\right], \tag{2.10}$$

$$\det DP_\Gamma(\eta,\xi) = \left\|\mathbf{g}'(\xi)\right\|\left(1+\eta\kappa(\xi)\right), \tag{2.11}$$

$$DR_\Gamma(x,y) = \begin{bmatrix}\mathbf{n}^T(\xi)\\ \left\|\mathbf{g}'(\xi)\right\|^{-1}\left(1+\eta\kappa(\xi)\right)^{-1}\boldsymbol{\tau}^T(\xi)\end{bmatrix}, \tag{2.12}$$

$$\det DR_\Gamma(x,y) = \left\|\mathbf{g}'(\xi)\right\|^{-1}\left(1+\eta\kappa(\xi)\right)^{-1}. \tag{2.13}$$

Here and below, (x,y) and (η,ξ) are related through (2.6) and (2.7). Since Γ is regular and C^2, there exist positive constants C_1, C_2, and C_3 such that

$$0 < C_1 \le \left\|\mathbf{g}'(\xi)\right\| \le C_2, \qquad \left\|\mathbf{g}''(\xi)\right\| \le C_2, \qquad |\kappa(\xi)| \le C_3, \quad \xi\in[\xi_s,\xi_e]. \tag{2.14}$$

The following lemma states uniform bounds for the Frenet transformations and their Jacobians.

Lemma 2.1. There exist constants $\epsilon_0 > 0$ and $\tilde{C}_J,\ C_J > 0$ such that, for every $0 < \epsilon \le \epsilon_0$,

$$\frac{1}{2} \le 1+\eta\kappa(\xi) \le 2, \qquad (\eta,\xi)\in[-\epsilon,\epsilon]\times[\xi_s,\xi_e], \tag{2.15}$$

$$\tilde{C}_J \le \left|\det DP_\Gamma(\eta,\xi)\right| \le C_J, \qquad \left\|DP_\Gamma(\eta,\xi)\right\| \le C_J, \quad (\eta,\xi)\in[-\epsilon,\epsilon]\times[\xi_s,\xi_e], \tag{2.16}$$

$$\tilde{C}_J \le \left|\det DR_\Gamma(x,y)\right| \le C_J, \qquad \left\|DR_\Gamma(x,y)\right\| \le C_J, \quad (x,y)\in N_\Gamma(\epsilon). \tag{2.17}$$

Proof. Choose $\epsilon_0 > 0$ so that $\epsilon_0 C_3 \le 1/2$. Then (2.15) follows immediately from (2.14). The determinant bounds follow from (2.11), (2.13), and the two-sided bound on $\left\|\mathbf{g}'\right\|$. The matrix-norm bounds follow from (2.10), (2.12), and (2.15). □

Without loss of generality, we assume ϵ is sufficiently small that the boundary and interface tubular neighborhoods are disjoint:

$$N_{\Gamma_b}(\epsilon)\cap N_{\Gamma_i}(\epsilon) = \emptyset,$$

and that, for $0<\epsilon\le\epsilon_0$, there exists $h_0 > 0$ such that

$$\bigcup_{K\in\mathcal{T}_h^c} K \subset N_{\Gamma_b}(\epsilon)\cup N_{\Gamma_i}(\epsilon), \qquad \bigcup_{K\in\mathcal{T}_h^i} K \subset N_{\Gamma_i}(\epsilon), \qquad h\le h_0. \tag{2.18}$$

Thus, every curved element or interface element lies in the tubular neighborhood of its associated curve. Unless stated otherwise, Γ denotes either Γ_b or Γ_i, as determined by the element under consideration.

2.3. **Projected curve segments.** For $K \in \mathcal{T}_h^c \cup \mathcal{T}_h^i$, define

$$\Xi_K := \{\xi(X) : X \in K\}, \qquad \xi_m(K) := \min \Xi_K, \qquad \xi_M(K) := \max \Xi_K, \tag{2.19}$$

and consider its orthogonal projection onto Γ:

$$\Gamma_{K,\mathrm{Proj}} := \{\mathbf{g}(\xi) : \xi_m(K) \le \xi \le \xi_M(K)\}. \tag{2.20}$$

The related vertex-based quantities are

$$\widehat{\Xi}_K := \{\xi(A_j) : j = 1,2,3\}, \qquad \widehat{\xi}_m(K) := \min \widehat{\Xi}_K, \qquad \widehat{\xi}_M(K) := \max \widehat{\Xi}_K, \tag{2.21}$$

and

$$\Gamma_{K,mM} := \{\mathbf{g}(\xi) : \widehat{\xi}_m(K) \le \xi \le \widehat{\xi}_M(K)\}. \tag{2.22}$$

Lemma 2.2. Assume that $0 < \epsilon \le \epsilon_0$ and (2.18) holds. Then

$$\Gamma_{K,\mathrm{Proj}} = \Gamma_{K,mM}$$

for every $K \in \mathcal{T}_h^c \cup \mathcal{T}_h^i$ with vertices A_1, A_2, and A_3.

Proof. Since $\nabla\xi \neq 0$ in $N_\Gamma(\epsilon)$, the function $\xi(X)$ has no interior local extremum in K. Hence its extrema over the element K are attained on ∂K because K is a compact set.

Each edge of K is either a segment of Γ or a straight line segment. On a curve edge, ξ is the curve parameter and is monotone. On a straight edge, the level sets of ξ are the normal segments $\{\mathbf{g}(\xi) + \eta\mathbf{n}(\xi) : |\eta| \le \epsilon\}$. A straight edge meets each such level set at most once unless it overlaps one, in which case ξ is constant on the overlap. Therefore, the restriction of ξ to each edge is monotone or constant, and its edgewise extrema occur at the endpoints. Consequently,

$$\xi_m(K) = \min_{1\le j\le 3} \xi(A_j) = \widehat{\xi}_m(K), \qquad \xi_M(K) = \max_{1\le j\le 3} \xi(A_j) = \widehat{\xi}_M(K).$$

The conclusion follows from (2.20) and (2.22). □

The next two lemmas show that the length of the projected curve segment is comparable to the element diameter.

Lemma 2.3. Under the assumptions of Lemma 2.2, there exists a constant C_u, independent of K and h, such that

$$|\Gamma_{K,\mathrm{Proj}}| \le C_u h_K, \qquad K \in \mathcal{T}_h^c \cup \mathcal{T}_h^i. \tag{2.23}$$

Proof. By (2.9), (2.14), and (2.15),

$$\|\nabla\xi(X)\| \le \frac{2}{C_1}, \qquad X \in N_\Gamma(\epsilon). \tag{2.24}$$

By Lemma 2.2, there exist vertices X_1, X_2 of K such that

$$\xi_m(K) = \xi(X_1), \qquad \xi_M(K) = \xi(X_2).$$

For h_0 sufficiently small, the segment $\overline{X_1X_2}$ lies in a fixed tubular neighborhood on which (2.24) holds. The mean value theorem therefore gives

$$|\xi_M(K) - \xi_m(K)| \le \sup_{X\in\overline{X_1X_2}} \|\nabla\xi(X)\|\, \|X_2 - X_1\| \le \frac{2}{C_1} h_K. \tag{2.25}$$

Therefore,

$$\left|\Gamma_{K,\mathrm{Proj}}\right| = \int_{\xi_m(K)}^{\xi_M(K)} \left\|\mathbf{g}'(\xi)\right\| \, d\xi \le C_2 \left|\xi_M(K) - \xi_m(K)\right| \le \frac{2C_2}{C_1} h_K.$$

Thus (2.23) holds with $C_u = 2C_2/C_1$. □

Lemma 2.4. Assume that $0 < \epsilon \le \epsilon_0$ and that (2.18) holds for h_0 sufficiently small. Then there exists a constant $C_l > 0$, independent of K and h, such that

$$\left|\Gamma_{K,\mathrm{Proj}}\right| \ge C_l h_K, \qquad K \in \mathcal{T}_h^c \cup \mathcal{T}_h^i. \tag{2.26}$$

Proof. Let $X_0 \in K$ be the center of an inscribed ball of radius ρ_K, so that $\overline{B}(X_0, \rho_K) \subset K$. Set $\xi_0 := \xi(X_0)$ and

$$X_+ := X_0 + \rho_K \boldsymbol{\tau}(\xi_0), \qquad X_- := X_0 - \rho_K \boldsymbol{\tau}(\xi_0).$$

Both points belong to K. For $X(t) := tX_+ + (1-t)X_-$, $0 \le t \le 1$, the segment $\{X(t) : 0 \le t \le 1\}$ lies in the inscribed ball and hence in K. Moreover, by (2.24) and (2.3),

$$|\xi(X(t)) - \xi_0| \le \frac{2}{C_1} \|X(t) - X_0\| \le \frac{2\rho_K}{C_1} \le C h_K.$$

Since $\boldsymbol{\tau}$ is uniformly continuous, for h_0 sufficiently small,

$$\boldsymbol{\tau}(\xi(X(t))) \cdot \boldsymbol{\tau}(\xi_0) \ge \frac{1}{2}, \qquad 0 \le t \le 1.$$

Using (2.9), (2.14), and (2.15), we obtain

$$\nabla\xi(X(t)) \cdot \boldsymbol{\tau}(\xi_0) = \frac{\boldsymbol{\tau}(\xi(X(t))) \cdot \boldsymbol{\tau}(\xi_0)}{\left\|\mathbf{g}'(\xi(X(t)))\right\| \left(1 + \eta(X(t))\kappa(\xi(X(t)))\right)} \ge \frac{1}{4C_2}.$$

Therefore,

$$\xi(X_+) - \xi(X_-) = 2\rho_K \int_0^1 \nabla\xi(X(t)) \cdot \boldsymbol{\tau}(\xi_0) \, dt, \tag{2.27}$$

$$\xi(X_+) - \xi(X_-) \ge \frac{\rho_K}{2C_2} \ge \frac{h_K}{2C_{\mathrm{sh}} C_2}. \tag{2.28}$$

In particular,

$$\xi_m(K) \le \xi(X_-) < \xi(X_+) \le \xi_M(K). \tag{2.29}$$

Finally,

$$\left|\Gamma_{K,\mathrm{Proj}}\right| = \int_{\xi_m(K)}^{\xi_M(K)} \left\|\mathbf{g}'(\xi)\right\| \, d\xi \ge C_1 \left(\xi_M(K) - \xi_m(K)\right) \ge \frac{C_1}{2C_{\mathrm{sh}} C_2} h_K. \tag{2.30}$$

This proves the result with $C_l = C_1/(2C_{\mathrm{sh}} C_2)$. □

2.4. **Fictitious elements and finite overlap.** For $K \in \mathcal{T}_h^c \cup \mathcal{T}_h^i$, define the fictitious element

$$K_F := P_\Gamma\big([-h_K, h_K] \times [\xi_m(K), \xi_M(K)]\big)$$

which is a curved quadrilateral bounded by the two curves

$$P_\Gamma(\pm h_K, \xi), \qquad \xi_m(K) \le \xi \le \xi_M(K),$$

and by the two normal segments through $\mathbf{g}(\xi_m(K))$ and $\mathbf{g}(\xi_M(K))$. Since every element in $\mathcal{T}_h^c \cup \mathcal{T}_h^i$ intersects its associated curve and has diameter h_K, we have $K \subset K_F$. Its image in Frenet coordinates is the rectangle

$$\widehat{K}_F := R_\Gamma(K_F) = [-h_K, h_K] \times [\xi_m(K), \xi_M(K)].$$

The curve segment $\Gamma_{K,\mathrm{Proj}}$ divides K_F into K_F^- and K_F^+, while its image $\widehat{\Gamma}_{K,\mathrm{Proj}}$ divides $\widehat{K}_F$ into $\widehat{K}_F^-$ and $\widehat{K}_F^+$. These sets are illustrated in Figure 2.

For $X \in \Omega$, define

$$\mathscr{F}_h(X) := \big\{K_F : X \in K_F,\ K \in \mathcal{T}_h^c \cup \mathcal{T}_h^i\big\}. \tag{2.31}$$

Lemma 2.5. Assume in addition that $\mathcal{T}_h$ is quasi-uniform. Then there exists a constant C, independent of h and X, such that

$$\sum_{K \in \mathcal{T}_h^c \cup \mathcal{T}_h^i} \chi_{K_F}(X) \le C, \qquad X \in \Omega. \tag{2.32}$$

Proof. For $X \in \Omega$, let $K_F \in \mathscr{F}_h(X)$. Since $\xi(X) \in [\xi_m(K), \xi_M(K)]$ and $\xi(K)$ is a connected interval, there exists $Y \in K$ such that $\xi(Y) = \xi(X)$. The element K intersects its associated curve Γ, so $\big|\eta(Y)\big| \le h_K$. By the definition of K_F, $\big|\eta(X)\big| \le h_K$. Since X and Y lie on the same normal segment,

$$\|X - Y\| = \big|\eta(X) - \eta(Y)\big| \le 2h_K \le 2h.$$

Hence every element associated with a member of $\mathscr{F}_h(X)$ intersects $B(X, 2h)$ and is contained in $B(X, 3h)$.

By shape regularity and quasi-uniformity, there is a constant $c > 0$ such that $|K| \ge ch^2$ for every $K \in \mathcal{T}_h$. Since the elements have disjoint interiors,

$$ch^2\, |\mathscr{F}_h(X)| \le \sum_{K_F \in \mathscr{F}_h(X)} |K| \le |B(X, 3h)| = 9\pi h^2.$$

Here, $|\mathscr{F}_h(X)|$ denotes the number of elements in the set $\mathscr{F}_h(X)$. Thus $|\mathscr{F}_h(X)| \le 9\pi/c$, which implies (2.32). □

2.5. **Norm equivalence under the Frenet transformation.** Let $D \subset N_\Gamma(\epsilon)$ be an open subset and set $\widehat{D} := R_\Gamma(D)$. For $v : D \to \mathbb{R}$, define $\widehat{v} := v \circ P_\Gamma$. If $v \in H^1(D)$, then $\widehat{v} \in H^1(\widehat{D})$ and

$$\nabla v = (DR_\Gamma)^T \widehat{\nabla} \widehat{v}, \qquad \widehat{\nabla} \widehat{v} = (DP_\Gamma)^T \nabla v. \tag{2.33}$$

The following lemma gives the equivalence of the L^2 norms of v and $\hat{v}$, and of their gradients.

Lemma 2.6. For $0 < \epsilon \le \epsilon_0$, there exists a constant C, independent of D and v, such that

$$C^{-1}\, \|v\|_{0,D} \le \|\widehat{v}\|_{0,\widehat{D}} \le C\, \|v\|_{0,D}, \qquad v \in L^2(D), \tag{2.34}$$

$$C^{-1}\, \|\nabla v\|_{0,D} \le \|\nabla \widehat{v}\|_{0,\widehat{D}} \le C\, \|\nabla v\|_{0,D}, \qquad v \in H^1(D). \tag{2.35}$$

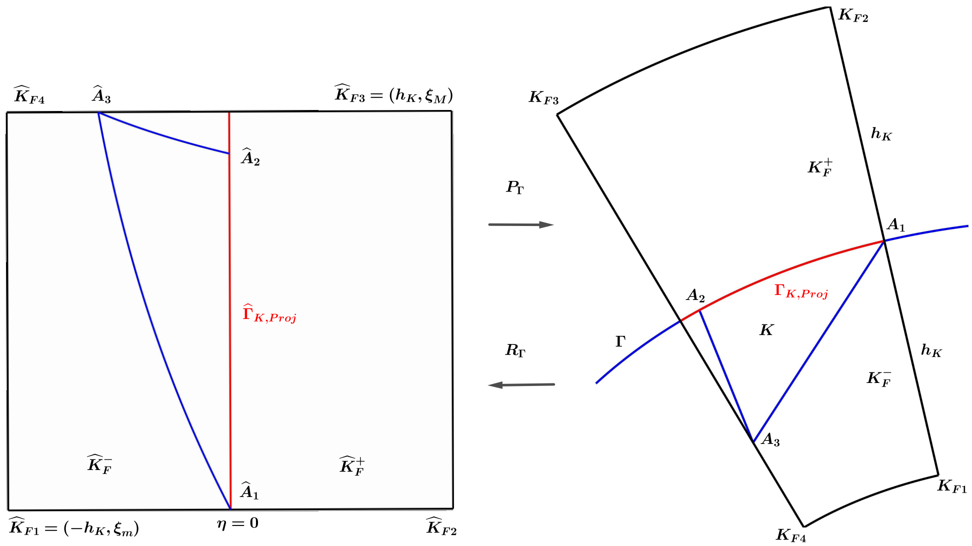

FIGURE 2. The mappings P_Γ and R_Γ between $K_F = K_F^- \cup K_F^+$ and $\widehat{K}_F = \widehat{K}_F^- \cup \widehat{K}_F^+$ for K associated with either a curved boundary or a fitted interface.

Proof. The change-of-variables formula and Lemma 2.1 give

$$\|v\|_{0,D}^2 = \int_{\widehat{D}} \widehat{v}(\eta,\xi)^2 \left|\det DP_\Gamma(\eta,\xi)\right| d\eta\, d\xi \simeq \|\widehat{v}\|_{0,\widehat{D}}^2.$$

Using (2.33), the uniform matrix bounds in Lemma 2.1, and the same change of variables yields

$$\|\nabla v\|_{0,D} \le C \left\|\widehat{\nabla}\widehat{v}\right\|_{0,\widehat{D}}, \qquad \left\|\widehat{\nabla}\widehat{v}\right\|_{0,\widehat{D}} \le C \|\nabla v\|_{0,D}.$$

This proves both assertions. □

Remark 1. The norm equivalences in Lemma 2.6 extend to higher Sobolev orders. If Γ is of class C^{m+2}, then there exists a constant $C \ge 1$ such that

$$C^{-1} \|v\|_{j,D} \le \|\widehat{v}\|_{j,\widehat{D}} \le C \|v\|_{j,D}, \qquad 0 \le j \le m+1.$$

The constants are uniform for $D \subset N_\Gamma(\epsilon)$ and fixed $0 < \epsilon \le \epsilon_0$. The result follows from repeated applications of the chain rule, the uniform bounds on the derivatives of P_Γ and R_Γ, and the determinant bounds in Lemma 2.1.

3. GEOMETRY-CONFORMING FINITE ELEMENT SPACES

In this section, $\{\mathcal{T}_h\}_{h>0}$ is a family of quasi-uniform, interface-fitted curved meshes in the sense of Section 2; hence, $\mathcal{T}_h^i = \emptyset$ and $\mathcal{T}_h = \mathcal{T}_h^c \cup \mathcal{T}_h^r$. We assume that the boundary and interface curves are of class C^{m+2} and that $h \le h_0$ is sufficiently small. For each $K \in \mathcal{T}_h^c$, let Γ denote the associated segment of either Γ_b or Γ_i. Let Ω_K be the physical subdomain containing K. The index $s_K \in \{+,-\}$ is such that

$$K \subset K_F^{s_K} \subset \Omega_K.$$

For a curved-boundary element K, Ω_K is the domain on the interior side of Γ_b, and for an interface-fitted element, it is either Ω^- or Ω^+. We begin with the construction of the geometry-conforming finite element space on $K \in \mathcal{T}_h^c$.

3.1. **Local and global GC-FE spaces.** Let p_s, $0 \le s \le m$, be the Legendre polynomial of degree s. For $0 \le t \le m$, let q_t be a polynomial of degree exactly t satisfying

$$q_0(x) = p_0(x) = 1, \qquad q_1(0) = 0, \qquad q_i(0) = q_i'(0) = 0, \quad 2 \le i \le m.$$

One particular family $\{q_t\}_{t=0}^m$ is given in [6]; other families satisfying these conditions may also be used. Let $K \in \mathcal{T}_h^c$ have vertices A_1, A_2, A_3, and write $(\eta_i, \xi_i) = R_\Gamma(A_i)$. Define

$$\eta_{h,K} := \max_{1\le i\le 3} |\eta_i|, \qquad \xi_K^{\mathtt{mid}} := \frac{\xi_m(K) + \xi_M(K)}{2}, \qquad \xi_{h,K} := \frac{\xi_M(K) - \xi_m(K)}{2}. \tag{3.1}$$

The nondegeneracy of K gives $\eta_{h,K} > 0$, and Lemmas 2.3 and 2.4, together with the uniform bounds on $\|\mathbf{g}'\|$, imply $\xi_{h,K} \simeq h_K$.

Set

$$\widehat{q}_t(\eta) := q_t\left(\frac{\eta}{\eta_{h,K}}\right), \qquad \widehat{p}_j(\xi) := p_j\left(\frac{\xi - \xi_K^{\mathtt{mid}}}{\xi_{h,K}}\right),$$

$$\widehat{\phi}_{k(t,j)}(\eta,\xi) := \widehat{q}_t(\eta)\widehat{p}_j(\xi), \qquad k(t,j) := \frac{(t+j)(t+j+1)}{2} + t + 1, \tag{3.2}$$

for $0 \le t \le m$ and $0 \le j \le m - t$. The index map $k(t,j)$ is the Cantor pairing function restricted to pairs with $t + j \le m$. Its inverse is

$$d(k) := \left\lfloor \frac{\sqrt{8k-7}-1}{2} \right\rfloor, \qquad t(k) := k - 1 - \frac{d(k)(d(k)+1)}{2}, \qquad s(k) := d(k) - t(k). \tag{3.3}$$

Because q_t and p_s have exact degrees t and s, respectively, the functions in (3.2) form a basis of the total-degree polynomial space:

$$\mathbb{P}_m(\widehat{K}_F^{s_K}) = \operatorname{span}\{\widehat{\phi}_k : 1 \le k \le (m+1)(m+2)/2\}. \tag{3.4}$$

Moreover,

$$\widehat{\phi}_k(0,\xi) = 0 \qquad \text{whenever } t(k) \ge 1. \tag{3.5}$$

Thus, only the modes with $t(k) = 0$ contribute to the trace on the physical curve $\eta = 0$.

We then define the GC-FE space on the physical-side fictitious element by

$$\begin{aligned} S_h^m(K_F^{s_K}) &:= \{\widehat{v} \circ R_\Gamma : \widehat{v} \in \mathbb{P}_m(\widehat{K}_F^{s_K})\} \\ &= \operatorname{span}\{\phi_k := \widehat{\phi}_k \circ R_\Gamma : 1 \le k \le (m+1)(m+2)/2\}. \end{aligned} \tag{3.6}$$

The local space on the curved element is the restriction

$$S_h^m(K) := \{v|_K : v \in S_h^m(K_F^{s_K})\} = \operatorname{span}\{\phi_k|_K\}, \qquad K \in \mathcal{T}_h^c. \tag{3.7}$$

Since a polynomial that vanishes on the set $R_\Gamma(K)$ vanishes identically, the restriction is injective and

$$\dim S_h^m(K) = \frac{(m+1)(m+2)}{2} =: d_m.$$

For $K \in \mathcal{T}_h^r$, set $S_h^m(K) := \mathbb{P}_m(K)$ as usual. The global GC-FE space is then defined as

$$S_h^m(\mathcal{T}_h) := \{v \in L^2(\Omega) : v|_K \in S_h^m(K) \text{ for every } K \in \mathcal{T}_h\}. \tag{3.8}$$

3.2. **GC-FE basis reconstruction.** The tensor-product-type basis $\{\widehat{\phi}_k : 1 \le k \le d_m\}$ defined in (3.2) is commonly used in finite element computation and analysis, but its associated local mass matrix can become increasingly ill-conditioned as the polynomial degree increases. Such ill-conditioning indicates that the basis functions are nearly linearly dependent and can amplify roundoff errors and degrade numerical stability. To improve the conditioning, we adapt the basis-reconstruction procedures developed for GC-IFE spaces in [6, 29].

To describe the basis reconstructions, let

$$\boldsymbol{\phi}_K := (\phi_1^K, \ldots, \phi_{d_m}^K)^T, \qquad \phi_j^K := (\widehat{\phi}_j \circ R_\Gamma)|_K,$$

be the original basis of the local GC-FE space $S_h^m(K)$ defined in (3.6), where $K \in \mathcal{T}_h^c$.

Choose a quadrature rule on K with nodes and positive weights $\{(X_r, w_r)\}_{r=1}^{N_q}$, and define

$$(\mathsf{V}_K)_{rj} := \phi_j^K(X_r), \qquad \mathsf{W}_K := \operatorname{diag}(w_1, \ldots, w_{N_q}), \qquad \mathsf{A}_K := \mathsf{W}_K^{1/2}\mathsf{V}_K.$$

Assume that $N_q \ge d_m$ and that A_K has full column rank. The quadrature-based local mass matrix is then

$$\mathsf{M}_{q,K} := \mathsf{V}_K^T \mathsf{W}_K \mathsf{V}_K = \mathsf{A}_K^T \mathsf{A}_K,$$

which is symmetric positive definite.

For any nonsingular matrix $\mathsf{Q} \in \mathbb{R}^{d_m \times d_m}$, the transformed functions $\widetilde{\boldsymbol{\phi}}_K := \mathsf{Q}^T \boldsymbol{\phi}_K$ form another basis of $S_h^m(K)$, whose quadrature-based mass matrix is

$$\widetilde{\mathsf{M}}_{q,K} = \mathsf{Q}^T \mathsf{M}_{q,K} \mathsf{Q}. \tag{3.9}$$

In the first reconstruction approach (RA1), let $\mathsf{M}_{q,K} = \mathsf{V}_1 \boldsymbol{\Lambda} \mathsf{V}_1^T$ be its spectral decomposition and set $\mathsf{Q}_1 := \mathsf{V}_1 \boldsymbol{\Lambda}^{-1/2}$, $\quad \widetilde{\boldsymbol{\phi}}_K^{(1)} := \mathsf{Q}_1^T \boldsymbol{\phi}_K$. It follows from (3.9) that $\widetilde{\mathsf{M}}_{q,K}^{(1)} = \mathsf{Q}_1^T \mathsf{M}_{q,K} \mathsf{Q}_1 = \mathsf{I}$. Thus, RA1 produces a basis orthonormal with respect to the quadrature inner product.

In the second reconstruction approach (RA2), we compute the reduced singular value decomposition $\mathsf{A}_K = \mathsf{U}_2 \boldsymbol{\Sigma} \mathsf{V}_2^T$ and set $\mathsf{Q}_2 := \mathsf{V}_2 \boldsymbol{\Sigma}^{-1}$, $\quad \widetilde{\boldsymbol{\phi}}_K^{(2)} := \mathsf{Q}_2^T \boldsymbol{\phi}_K$. Again, by (3.9), we have $\widetilde{\mathsf{M}}_{q,K}^{(2)} = \mathsf{Q}_2^T \mathsf{M}_{q,K} \mathsf{Q}_2 = \mathsf{I}$.

Thus, in exact arithmetic, both RA1 and RA2 produce bases orthonormal with respect to the quadrature inner product and hence identity quadrature-based mass matrices, although the reconstructed bases may differ by an orthogonal transformation. In finite precision, however, because

$$\operatorname{cond}_2(\mathsf{M}_{q,K}) = \operatorname{cond}_2(\mathsf{A}_K)^2,$$

computing the SVD used by RA2 is generally less susceptible to roundoff error. The numerical comparison in Subsection 5.1 also corroborates the greater robustness of RA2 for high polynomial degrees. The reconstruction changes only the basis, not the local GC-FE space, and therefore does not affect the approximation or stability analysis below. Accordingly, we recommend the basis produced by RA2 for GC-FE computations.

3.3. **Projection operators and approximation estimates.** For $K \in \mathcal{T}_h^c$, let

$$\widehat{\Pi}_{\widehat{K}_F^{s_K}} : L^2(\widehat{K}_F^{s_K}) \longrightarrow \mathbb{P}_m(\widehat{K}_F^{s_K})$$

be the standard L^2 projection, which is characterized by

$$\big(\widehat{\Pi}_{\widehat{K}_F^{s_K}} \widehat{u}, \widehat{v}\big)_{0,\widehat{K}_F^{s_K}} = \big(\widehat{u}, \widehat{v}\big)_{0,\widehat{K}_F^{s_K}} \qquad \forall \widehat{v} \in \mathbb{P}_m(\widehat{K}_F^{s_K}). \tag{3.10}$$

For $u \in L^2(K_F^{s_K})$, set $\widehat{u} := u \circ P_\Gamma$ and define the Frenet *pullback* projection

$$\Pi_{K_F^{s_K}} u := \big(\widehat{\Pi}_{\widehat{K}_F^{s_K}} \widehat{u}\big) \circ R_\Gamma. \tag{3.11}$$

The corresponding local operator is defined as

$$\Pi_K u := \big(\Pi_{K_F^{s_K}} (u|_{K_F^{s_K}})\big)|_K, \qquad K \in \mathcal{T}_h^c. \tag{3.12}$$

For $K \in \mathcal{T}_h^r$, Π_K is the usual $L^2(K)$ projection onto $\mathbb{P}_m(K)$. Finally, define $\Pi_h : L^2(\Omega) \to S_h^m(\mathcal{T}_h)$ elementwise by

$$(\Pi_h u)|_K := \Pi_K u, \qquad K \in \mathcal{T}_h. \tag{3.13}$$

We first estimate the local projection error on a curved element $K \in \mathcal{T}_h^c$.

Lemma 3.1. For every $K \in \mathcal{T}_h^c$ and every $u \in H^{m+1}(K_F^{s_K})$, there exists a constant C, independent of K and h, such that

$$|\Pi_K u - u|_{k,K} \le C h_K^{m+1-k} \, \|u\|_{m+1,K_F^{s_K}}, \qquad 0 \le k \le m+1. \tag{3.14}$$

Proof. Note that $\widehat{K}_F^{s_K}$ is a rectangle and its side in the η-direction has length h_K. Lemmas 2.3 and 2.4, together with the uniform bounds on $\|\mathbf{g}'\|$, show that its side in the ξ-direction has a length comparable to h_K. Thus these rectangles form a uniformly shape-regular family after scaling by h_K.

The standard approximation estimate for the L^2 projection onto $\mathbb{P}_m(\widehat{K}_F^{s_K})$ gives

$$\Big|\widehat{\Pi}_{\widehat{K}_F^{s_K}} \widehat{u} - \widehat{u}\Big|_{k,\widehat{K}_F^{s_K}} \le C h_K^{m+1-k} \, \|\widehat{u}\|_{m+1,\widehat{K}_F^{s_K}}, \qquad 0 \le k \le m+1. \tag{3.15}$$

The higher-order norm equivalence in Remark 1 transfers this estimate to $K_F^{s_K}$. Restricting the result to $K \subset K_F^{s_K}$ proves (3.14). □

Lemma 3.1 can be extended to functions of lower regularity as described in the following corollary.

Corollary 3.1. Let $K \in \mathcal{T}_h^c$, and choose $s_K \in \{+,-\}$ so that

$$K \subset K_F^{s_K} \subset \Omega_K. \tag{3.16}$$

Let $2 \le r \le m+1$ and $0 \le j \le \min\{r, 2\}$. Then there exists a constant C independent of K and h such that

$$|\Pi_K v - v|_{j,K} \le C h_K^{r-j} \, \|v\|_{r,K_F^{s_K}}, \qquad v \in H^r(K_F^{s_K}). \tag{3.17}$$

For $K \in \mathcal{T}_h^r$, the same estimate holds with $K_F^{s_K}$ replaced by K.

Proof. The result follows from the proof of Lemma 3.1, applied with regularity index r. The inclusion $K_F^{s_K} \subset \Omega_K$ ensures that the relevant Sobolev norm is taken over a single smooth physical subdomain. For $K \in \mathscr{T}_h^r$, the result reduces to the standard polynomial projection estimate. □

For a piecewise H^k function, set

$$|w|_{k,\mathscr{T}_h}^2 := \sum_{K\in\mathscr{T}_h} |w|_{k,K}^2.$$

The following theorem gives the global approximation property of $S_h^m(\mathscr{T}_h)$.

Theorem 3.1. There exists a constant C, independent of h, such that for $0 \le k \le m+1$

$$|\Pi_h u - u|_{k,\mathscr{T}_h} \le C h^{m+1-k} \|u\|_{m+1,\Omega}, \qquad u \in H^{m+1}(\Omega). \tag{3.18}$$

Proof. Lemma 3.1 and the standard polynomial projection estimate on $K \in \mathscr{T}_h^r$ yield

$$|\Pi_h u - u|_{k,\mathscr{T}_h}^2 \le C h^{2(m+1-k)} \left(\sum_{K\in\mathscr{T}_h^c} \|u\|_{m+1,K_F^{s_K}}^2 + \sum_{K\in\mathscr{T}_h^r} \|u\|_{m+1,K}^2 \right).$$

Since $K_F^{s_K} \subset K_F$, the finite-overlap estimate of Lemma 2.5 gives

$$\sum_{K\in\mathscr{T}_h^c} \|u\|_{m+1,K_F^{s_K}}^2 \le \sum_{|\alpha|\le m+1} \int_\Omega \left|D^\alpha u(X)\right|^2 \left(\sum_{K\in\mathscr{T}_h^c} \chi_{K_F}(X) \right) dX \le C \|u\|_{m+1,\Omega}^2.$$

Combining the last two estimates and taking square roots proves (3.18). □

Remark 2. The same proof applies to functions that are only piecewise smooth across a fitted interface. More precisely, if $u|_{\Omega^\pm} \in H^{m+1}(\Omega^\pm)$, then the estimate (3.18) can be replaced by

$$|\Pi_h u - u|_{k,\mathscr{T}_h} \le C h^{m+1-k} \left(\|u\|_{m+1,\Omega^-}^2 + \|u\|_{m+1,\Omega^+}^2 \right)^{1/2}.$$

3.4. **Inverse estimates.** Although GC-FE functions are generally nonpolynomial in Cartesian coordinates, their pullbacks belong to a polynomial space of prescribed degree. This polynomial structure of their pullbacks further ensures that GC-FE functions satisfy the inverse estimates stated below.

Theorem 3.2. Assume that the parametrization of Γ is of class C^3. There exists a constant C, independent of K and h, such that

$$|v_h|_{j,K} \le C h_K^{\ell-j} |v_h|_{\ell,K}, \qquad 0 \le \ell \le j \le 2, \qquad v_h \in S_h^m(K),\ K \in \mathscr{T}_h. \tag{3.19}$$

The constant may depend on the fixed polynomial degree m and the mesh and geometric regularity constants.

Proof. The result is standard for $K \in \mathscr{T}_h^r$. Let $K \in \mathscr{T}_h^c$, set $\widehat{K} := R_\Gamma(K)$, and write $v_h = \widehat{v}_h \circ R_\Gamma$ with $\widehat{v}_h \in \mathbb{P}_m$. The uniform bounds for P_Γ and R_Γ, together with the shape regularity of K, imply the existence of constants $c, C > 0$ and points $\widehat{X}_K$ such that

$$B(\widehat{X}_K, c h_K) \subset \widehat{K} \subset B(\widehat{X}_K, C h_K).$$

After translation and scaling by h_K, finite-dimensional norm equivalence on $\mathbb{P}_m$ and the usual polynomial inverse estimate therefore give

$$|\widehat{v}_h|_{j,\widehat{K}} \le C h_K^{\ell-j} |\widehat{v}_h|_{\ell,\widehat{K}}, \qquad 0 \le \ell \le j \le 2. \tag{3.20}$$

The first-derivative chain rule and Lemma 2.6 yield $|v_h|_{1,K} \le C h_K^{-1} \|v_h\|_{0,K}$. For second derivatives, the chain rule gives

$$|v_h|_{2,K} \le C\big(|\widehat{v}_h|_{2,\widehat{K}} + |\widehat{v}_h|_{1,\widehat{K}}\big) \le C h_K^{-1} |v_h|_{1,K},$$

where $h_K \le h_0$ and the C^3 regularity provides uniform bounds for the second derivatives of R_Γ. The case $(\ell, j) = (0,2)$ follows by combining the last two estimates; the remaining cases follow immediately. □

3.5. **Trace estimates.** For a straight element $K \in \mathscr{T}_h^r$, the standard scaled trace inequality is

$$\|v\|_{0,\partial K}^2 \le C\left(h_K^{-1} \|v\|_{0,K}^2 + h_K |v|_{1,K}^2\right), \qquad v \in H^1(K). \tag{3.21}$$

We now establish the corresponding result for curved elements.

Let $K \in \mathscr{T}_h^c$ have curved edge $e_K = \widehat{A_1 A_2}$ with endpoints A_1 and A_2, and let A_3 be its third vertex. Let $\xi_i := \xi(A_i)$, $i = 1,2$, and let the parameterization of the curved edge be

$$\breve{\mathbf{g}}(t) := \mathbf{g}\big(\xi_1 + t(\xi_2 - \xi_1)\big), \qquad 0 \le t \le 1.$$

Thus, $\breve{\mathbf{g}}(0) = \mathbf{g}(\xi_1) = A_1$, $\breve{\mathbf{g}}(1) = \mathbf{g}(\xi_2) = A_2$. Since $|\xi_2 - \xi_1| \simeq h_K$, the uniform bound on $\mathbf{g}''$ gives

$$\big\|\breve{\mathbf{g}}''(t)\big\| \le C h_K^2, \qquad 0 \le t \le 1. \tag{3.22}$$

Let $\overline{K} := \triangle A_1 A_2 A_3$ be the straight triangle with vertices A_1, A_2, A_3, and let $\widehat{\overline{K}}$ be the reference triangle with vertices $\hat{A}_1 = (0,0)$, $\hat{A}_2 = (1,0)$, and $\hat{A}_3 = (0,1)$. Define the following blending-function mapping: $F_K : \widehat{\overline{K}} \to K$ such that

$$X = F_K(\hat{X}) = \overline{F}_K(\hat{X}) + \widehat{\phi}_K(\hat{X})$$

where $\overline{F}_K : \widehat{\overline{K}} \to \overline{K}$ is the standard affine mapping on a triangle such that

$$\overline{F}_K(\hat{X}) = B_K \hat{X} + A_1,\ B_K = [A_2 - A_1, A_3 - A_1],\ \forall \hat{X} \in \widehat{\overline{K}},$$

and $\widehat{\phi}_K(\hat{X})$ is a Gordon-Hall type blending extension function [13,14]:

$$\widehat{\phi}_K(\hat{X}) = \widehat{\phi}_K(\hat{x}, \hat{y}) = \frac{1 - \hat{x} - \hat{y}}{1 - \hat{x}}\Big(\breve{\mathbf{g}}(\hat{x}) - \big(A_1 + \hat{x}(A_2 - A_1)\big)\Big), \qquad \forall \hat{X} = (\hat{x}, \hat{y}) \in \widehat{\overline{K}}.$$

By direct calculation, we have

$$DF_K(\hat{X}) = B_K + D\widehat{\phi}_K(\hat{X}) = B_K\left(I + B_K^{-1} D\widehat{\phi}_K(\hat{X})\right). \tag{3.23}$$

Since $\mathscr{T}_h$ is shape-regular, there exists a constant C such that

$$\|B_K\| \le C h_K, \quad \|B_K^{-1}\| \le C h_K^{-1}, \quad |\det B_K| \approx h_K^2. \tag{3.24}$$

The following lemma establishes a few essential estimates about the map F_K.

Lemma 3.2. There exists $h_0 > 0$ such that for every $K \in \mathscr{T}_h^c$, $h \le h_0$, $DF_K(\hat{X})$ is nonsingular, and the following hold for a certain constant C:

$$\begin{aligned} &\left|\det DF_K(\hat{X})\right| \le Ch_K^2, \quad \left|\det(DF_K(\hat{X}))^{-1}\right| \le Ch_K^{-2}, \\ &\left\|DF_K(\hat{X})\right\| \le Ch_K, \quad \left\|(DF_K(\hat{X}))^{-1}\right\| \le Ch_K^{-1}. \end{aligned} \tag{3.25}$$

Proof. By (3.22), we can show that there exists a constant C such that

$$\left\|\widehat{\phi}_K(\hat{X})\right\| \le Ch_K^2, \quad \left\|D\widehat{\phi}_K(\hat{X})\right\| \le Ch_K^2.$$

Then, by (3.24), $\|B_K^{-1}D\widehat{\phi}_K(\hat{X})\| \le \|B_K^{-1}\|\|D\widehat{\phi}_K(\hat{X})\| \le Ch_K^{-1}\cdot h_K^2 = Ch_K$. Therefore, by (3.23), there exists $h_0 > 0$ such that, whenever $h_K \le h \le h_0$, $DF_K(\hat{X})$ is nonsingular, and the estimates in (3.25) follow from direct calculations. $\square$

Consequently, for every edge $\widehat{e}$ of $\widehat{\widehat{K}}$ and every nonnegative measurable function f on its image $e = F_K(\widehat{e})$, we have

$$\int_e f\,ds \le Ch_K \int_{\widehat{e}} (f\circ F_K)\,d\widehat{s}. \tag{3.26}$$

Theorem 3.3. There exists $h_0 > 0$ and a constant C, independent of K and h, such that

$$\|v\|_{0,\partial K}^2 \le C\left(h_K^{-1}\|v\|_{0,K}^2 + h_K|v|_{1,K}^2\right), \qquad v \in H^1(K), \quad K \in \mathscr{T}_h, \quad h \le h_0. \tag{3.27}$$

Proof. For $K \in \mathscr{T}_h^r$, this is (3.21). Let $K \in \mathscr{T}_h^c$ and set $\widehat{v} := v\circ F_K$. Summing (3.26) over the three edges and applying the trace theorem on the fixed reference triangle gives

$$\|v\|_{0,\partial K}^2 \le Ch_K\|\widehat{v}\|_{0,\partial\widehat{\widehat{K}}}^2 \le Ch_K\left(\|\widehat{v}\|_{0,\widehat{\widehat{K}}}^2 + |\widehat{v}|_{1,\widehat{\widehat{K}}}^2\right).$$

By Lemma 3.2 and a change of variables,

$$\|\widehat{v}\|_{0,\widehat{\widehat{K}}}^2 \le Ch_K^{-2}\|v\|_{0,K}^2, \qquad |\widehat{v}|_{1,\widehat{\widehat{K}}}^2 \le C|v|_{1,K}^2.$$

Substituting into the inequality above proves (3.27). $\square$

Applying Theorem 3.3 componentwise to the gradient and then using the inverse estimates for GC-FE functions yields the following gradient and normal-flux trace estimates.

Corollary 3.2. There exists a constant C, independent of K and h, such that

$$\|\nabla v\|_{0,\partial K}^2 \le C\left(h_K^{-1}|v|_{1,K}^2 + h_K|v|_{2,K}^2\right), \qquad v \in H^2(K), \quad K \in \mathscr{T}_h. \tag{3.28}$$

Moreover, for every $v_h \in S_h^m(K)$,

$$\|\nabla v_h\|_{0,\partial K}^2 \le Ch_K^{-1}|v_h|_{1,K}^2, \qquad K \in \mathscr{T}_h, \tag{3.29}$$

and consequently

$$\|\nabla v_h\cdot\mathbf{n}_K\|_{0,\partial K}^2 \le Ch_K^{-1}|v_h|_{1,K}^2. \tag{3.30}$$

Proof. Applying Theorem 3.3 to each component of ∇v and summing the resulting inequalities gives (3.28). For $v_h \in S_h^m(K)$, the inverse estimate $|v_h|_{2,K} \le Ch_K^{-1}|v_h|_{1,K}$ then yields (3.29). Finally, (3.30) follows from $|\nabla v_h\cdot\mathbf{n}_K| \le |\nabla v_h|$ on ∂K. $\square$

4. An SIPDG Method with GC-FE Spaces: Formulation and Error Analysis

In this section, we employ GC-FE spaces in a standard symmetric interior penalty discontinuous Galerkin (SIPDG) formulation to solve the interface problem (1.3)–(1.5). We then establish a priori error estimates for the resulting SIPDG-GC-FE method. Owing to the geometry-conforming property of the GC-FE spaces, the error analysis does not require the treatment of geometric *variational crimes* arising in higher-degree finite element methods based on approximate geometries.

4.1. SIPDG method for the interface problem.

We consider the variable-coefficient interface problem (1.3)–(1.5) [22, 33], where

$$\beta|_{\Omega^\pm} = \beta^\pm \in W^{1,\infty}(\Omega^\pm), \qquad 0 < \underline{\beta} \le \beta^\pm \le \overline{\beta} < \infty \quad \text{a.e. in } \Omega^\pm.$$

For $s > 3/2$, let

$$\mathscr{H}^s(\Omega) := \left\{ v \in L^2(\Omega) : v|_{\Omega^\pm} \in H^s(\Omega^\pm) \right\}, \qquad H^s(\mathscr{T}_h) := \left\{ v \in L^2(\Omega) : v|_K \in H^s(K)\ \forall K \in \mathscr{T}_h \right\},$$

equipped with their usual broken Sobolev norms. Since the mesh is interface-fitted, each element is contained in the closure of one physical subdomain, and hence $\mathscr{H}^s(\Omega) \subset H^s(\mathscr{T}_h)$.

Let $\mathscr{E}_h$ be the set of mesh edges and set

$$\mathscr{E}_h^b := \{e \in \mathscr{E}_h : e \subset \Gamma_b\}, \qquad \mathscr{E}_h^\circ := \mathscr{E}_h \setminus \mathscr{E}_h^b, \qquad \mathscr{E}_h^\Gamma := \{e \in \mathscr{E}_h^\circ : e \subset \Gamma_i\}.$$

The curved edges are precisely those in $\mathscr{E}_h^\Gamma \cup \mathscr{E}_h^b$. For each $e \in \mathscr{E}_h$, fix a unit normal $\mathbf{n}_e$, chosen outward on boundary edges. If $e = \partial K_1 \cap \partial K_2$, orient $\mathbf{n}_e$ from K_1 to K_2 and define

$$[\![v]\!]_e := v_1 - v_2, \qquad \{\!\{v\}\!\}_e := \frac{1}{2}(v_1 + v_2).$$

On boundary edges, both operators denote the one-sided trace. On curved edges, $\mathbf{n}_e$ is understood pointwise. These conventions agree with the standard SIPDG conventions in [31].

For $w, v \in H^s(\mathscr{T}_h)$, define

$$\begin{aligned} a_h(w,v) = &\sum_{K \in \mathscr{T}_h} (\beta \nabla w, \nabla v)_K - \sum_{e \in \mathscr{E}_h} \left\langle \{\!\{\beta \partial_{\mathbf{n}_e} w\}\!\}_e, [\![v]\!]_e \right\rangle_e \\ &- \sum_{e \in \mathscr{E}_h} \left\langle \{\!\{\beta \partial_{\mathbf{n}_e} v\}\!\}_e, [\![w]\!]_e \right\rangle_e + \sum_{e \in \mathscr{E}_h} \frac{\sigma_0 \gamma_e}{h_e} \left\langle [\![w]\!]_e, [\![v]\!]_e \right\rangle_e, \end{aligned} \tag{4.1}$$

and

$$L_h(v) = (f, v)_\Omega + \sum_{e \in \mathscr{E}_h^b} \left\langle g, -\beta \partial_{\mathbf{n}_e} v + \frac{\sigma_0 \gamma_e}{h_e} v \right\rangle_e.$$

Here,

$$h_e = |e|, \qquad \beta_K := \operatorname*{ess\,sup}_{x \in K} \beta(x), \qquad \beta_e := \max_{K : e \subset \partial K} \beta_K, \qquad \gamma_e = m(m+1)\beta_e,$$

and $\sigma_0 > 0$ is the penalty parameter specified below.

Recall that the global GC-FE space defined in (3.8) satisfies $S_h^m(\mathscr{T}_h) \subset H^{m+1}(\mathscr{T}_h)$. The SIPDG-GC-FE method is to find $u_h \in S_h^m(\mathscr{T}_h)$ such that

$$a_h(u_h, v_h) = L_h(v_h) \qquad \forall v_h \in S_h^m(\mathscr{T}_h). \tag{4.2}$$

4.2. **A priori error analysis for the SIPDG-GC-FE method.** For $v \in H^s(\mathcal{T}_h)$, define the following norms:

$$\|v\|_{h,\beta}^2 = \sum_{K \in \mathcal{T}_h} \left\|\beta^{1/2}\nabla v\right\|_{0,K}^2 + \sum_{e \in \mathcal{E}_h} \left\| \left(\frac{\sigma_0 \gamma_e}{h_e}\right)^{1/2} [\![v]\!]_e \right\|_{0,e}^2, \tag{4.3}$$

$$|\!|\!| v |\!|\!|_{h,\beta}^2 = \|v\|_{h,\beta}^2 + \sum_{e \in \mathcal{E}_h} \left\| \left(\frac{h_e}{\sigma_0 \gamma_e}\right)^{1/2} \{\!\{\beta \partial_{\mathbf{n}_e} v\}\!\}_e \right\|_{0,e}^2. \tag{4.4}$$

In what follows, $C > 0$ denotes a generic constant independent of h; it may depend on the fixed degree m, the penalty parameter σ_0, the coefficient bounds, and the mesh and geometric regularity constants. For nonnegative quantities, $a \simeq b$ means $C^{-1}a \le b \le Ca$. For every adjacent edge–element pair $e \subset \partial K$, mesh regularity gives $h_e \simeq h_K$; for curved edges, this follows from Lemma 3.2. Moreover, $\underline{\beta} \le \beta_K \le \beta_e \le \overline{\beta}$. Since $\gamma_e = m(m+1)\beta_e$,

$$\frac{\sigma_0 \gamma_e}{h_e} \le C \frac{\sigma_0}{h_K}, \qquad \frac{h_e \beta_K^2}{\sigma_0 \gamma_e} \le C \frac{h_K \beta_K}{\sigma_0},$$

where the constants in these two estimates are independent of both h and σ_0.

Lemma 4.1. Let Π_h be the elementwise projection defined in (3.13). Assume that Γ_b and Γ_i are of class C^{m+2}, and that $\mathcal{T}_h$ is quasi-uniform with $h \le h_0$. For every integer r with $2 \le r \le m+1$ and every $v \in \mathcal{H}^r(\Omega)$, we have

$$\sum_{K \in \mathcal{T}_h} |v - \Pi_h v|_{j,K}^2 \le C h^{2(r-j)} \|v\|_{\mathcal{H}^r(\Omega)}^2, \qquad j = 0, 1, 2. \tag{4.5}$$

Moreover,

$$\sum_{K \in \mathcal{T}_h} \left(h_K^{-1} \|v - \Pi_h v\|_{0,\partial K}^2 + h_K \|\nabla(v - \Pi_h v)\|_{0,\partial K}^2 \right) \le C h^{2(r-1)} \|v\|_{\mathcal{H}^r(\Omega)}^2. \tag{4.6}$$

Proof. The estimate in (4.5) follows from the standard polynomial projection estimate on $K \in \mathcal{T}_h^r$ and Corollary 3.1 for $K \in \mathcal{T}_h^c$.

Applying Theorem 3.3 to $v - \Pi_h v$ and its derivatives yields

$$\|v - \Pi_h v\|_{0,\partial K}^2 \le C \left(h_K^{-1} \|v - \Pi_h v\|_{0,K}^2 + h_K |v - \Pi_h v|_{1,K}^2 \right).$$

$$\|\nabla(v - \Pi_h v)\|_{0,\partial K}^2 \le C \left(h_K^{-1} |v - \Pi_h v|_{1,K}^2 + h_K |v - \Pi_h v|_{2,K}^2 \right).$$

The estimate (4.6) follows from summing over these inequalities and using quasi-uniformity together with (4.5). □

Lemma 4.2. Under the assumptions of Lemma 4.1, for every integer r with $2 \le r \le m+1$ and every $v \in \mathcal{H}^r(\Omega)$,

$$|\!|\!| v - \Pi_h v |\!|\!|_{h,\beta} \le C h^{r-1} \|v\|_{\mathcal{H}^r(\Omega)}. \tag{4.7}$$

Proof. The coefficient bound and (4.5) with $j = 1$ give

$$\sum_{K \in \mathcal{T}_h} \left\|\beta^{1/2}\nabla(v - \Pi_h v)\right\|_{0,K}^2 \le C h^{2(r-1)} \|v\|_{\mathcal{H}^r(\Omega)}^2. \tag{4.8}$$

The edge-scale and weight relations above, the interior-edge average, the one-sided boundary convention, and the uniformly bounded number of edges per element imply

$$\sum_{e\in\mathcal{E}_h}\left\|\left(\frac{\sigma_0\gamma_e}{h_e}\right)^{1/2}[\![v-\Pi_h v]\!]_e\right\|_{0,e}^2+\sum_{e\in\mathcal{E}_h}\left\|\left(\frac{h_e}{\sigma_0\gamma_e}\right)^{1/2}\{\!\{\beta\partial_{\mathbf{n}}(v-\Pi_h v)\}\!\}_e\right\|_{0,e}^2$$
$$\le C\sum_{K\in\mathcal{T}_h}\left(h_K^{-1}\|v-\Pi_h v\|_{0,\partial K}^2+h_K\|\nabla(v-\Pi_h v)\|_{0,\partial K}^2\right)\le Ch^{2(r-1)}\|v\|_{\mathcal{H}^r(\Omega)}^2. \tag{4.9}$$

The estimate (4.7) follows from combining (4.8) and (4.9). □

Lemma 4.3. Assume that the parametrizations of Γ_b and Γ_i in (2.1) are of class C^3, and that $h\le h_0$. Then there exists a constant $C_{\mathrm{it}}>0$, independent of h and σ_0, such that

$$\sum_{e\in\mathcal{E}_h}\left\|\left(\frac{h_e}{\sigma_0\gamma_e}\right)^{1/2}\{\!\{\beta\partial_{\mathbf{n}}v_h\}\!\}_e\right\|_{0,e}^2\le\frac{C_{\mathrm{it}}}{\sigma_0}\sum_{K\in\mathcal{T}_h}\left\|\beta^{1/2}\nabla v_h\right\|_{0,K}^2,\qquad v_h\in S_h^m(\mathcal{T}_h). \tag{4.10}$$

This constant may depend on the fixed degree m, the ratio $\overline{\beta}/\underline{\beta}$, and the mesh and geometric regularity constants.

Proof. Applying Theorem 3.3 to the Cartesian derivatives of $v_h|_K$, and then using Theorem 3.2 with $(\ell,j)=(1,2)$, gives

$$\|\nabla v_h\cdot\mathbf{n}_K\|_{0,\partial K}^2\le\|\nabla v_h\|_{0,\partial K}^2\le C\left(h_K^{-1}|v_h|_{1,K}^2+h_K|v_h|_{2,K}^2\right)\le Ch_K^{-1}|v_h|_{1,K}^2.$$

For $e\in\mathcal{E}_h$, let ω_e be the set of elements adjacent to e. The interior-edge average and the one-sided boundary convention yield

$$\left|\{\!\{\beta\partial_{\mathbf{n}}v_h\}\!\}_e\right|^2\le C\sum_{K\in\omega_e}\beta_K^2|\partial_{\mathbf{n}}(v_h|_K)|^2.$$

Using the second edge-weight relation above and the fact that the edgewise normal $\mathbf{n}$ agrees with $\mathbf{n}_K$ up to sign on $e\subset\partial K$, we obtain

$$\sum_{e\in\mathcal{E}_h}\left\|\left(\frac{h_e}{\sigma_0\gamma_e}\right)^{1/2}\{\!\{\beta\partial_{\mathbf{n}}v_h\}\!\}_e\right\|_{0,e}^2\le\frac{C\overline{\beta}}{\sigma_0}\sum_{K\in\mathcal{T}_h}h_K\|\nabla v_h\cdot\mathbf{n}_K\|_{0,\partial K}^2.$$

The local estimate above and $\beta\ge\underline{\beta}$ then give

$$\sum_{e\in\mathcal{E}_h}\left\|\left(\frac{h_e}{\sigma_0\gamma_e}\right)^{1/2}\{\!\{\beta\partial_{\mathbf{n}}v_h\}\!\}_e\right\|_{0,e}^2\le\frac{C\overline{\beta}}{\sigma_0}\sum_{K\in\mathcal{T}_h}|v_h|_{1,K}^2\le\frac{C}{\sigma_0}\frac{\overline{\beta}}{\underline{\beta}}\sum_{K\in\mathcal{T}_h}\left\|\beta^{1/2}\nabla v_h\right\|_{0,K}^2.$$

Absorbing the fixed factors into C_{it} proves (4.10). □

Lemma 4.4. Let $s>3/2$. There exists a constant $C>0$, independent of h, such that

$$|a_h(w,v)|\le C|\!|\!|w|\!|\!|_{h,\beta}|\!|\!|v|\!|\!|_{h,\beta},\qquad w,v\in H^s(\mathcal{T}_h). \tag{4.11}$$

Suppose, in addition, that the assumptions of Lemma 4.3 hold, and let C_{it} be the constant in (4.10). Then

$$|a_h(w,v_h)|\le C\left(1+\frac{C_{\mathrm{it}}}{\sigma_0}\right)^{1/2}|\!|\!|w|\!|\!|_{h,\beta}\|v_h\|_{h,\beta},\qquad w\in H^s(\mathcal{T}_h),\quad v_h\in S_h^m(\mathcal{T}_h). \tag{4.12}$$

Furthermore, if $\sigma_0 \geq \sigma_* := 4C_{\mathrm{it}}$, then

$$a_h(v_h, v_h) \geq \frac{1}{2} \| v_h \|_{h,\beta}^2, \qquad v_h \in S_h^m(\mathcal{T}_h). \tag{4.13}$$

Consequently, the discrete problem (4.2) admits a unique solution.

Proof. Following the standard SIPDG argument [31], Cauchy–Schwarz applied to the element and edge terms of a_h gives (4.11). For $v_h \in S_h^m(\mathcal{T}_h)$, Lemma 4.3 controls the flux part of $|||v_h|||_{h,\beta}^2$ by C_{it}/σ_0 times its volume part, which gives (4.12).

Applying the same estimate and $2ab \leq \frac{1}{2}a^2 + 2b^2$ to the two symmetric flux terms in $a_h(v_h, v_h)$ gives (4.13) whenever $\sigma_0 \geq 4C_{\mathrm{it}}$. Finally, the one-sided boundary jump convention makes $\|\cdot\|_{h,\beta}$ a norm on $S_h^m(\mathcal{T}_h)$; coercivity and finite dimensionality therefore give existence and uniqueness. □

Lemma 4.5. Let $u \in \mathcal{H}^2(\Omega)$ solve (1.3)–(1.5) and let $u_h \in S_h^m(\mathcal{T}_h)$ solve (4.2). Then the following Galerkin orthogonality holds:

$$a_h(u - u_h, v_h) = 0, \qquad \forall\, v_h \in S_h^m(\mathcal{T}_h). \tag{4.14}$$

Proof. Elementwise integration by parts, together with the single-valued normal-flux trace on ordinary interior edges and the second interface jump condition on $\mathcal{E}_h^\Gamma$, gives

$$a_h(u, v_h) = L_h(v_h), \qquad \forall\, v_h \in S_h^m(\mathcal{T}_h),$$

where $[\![u]\!]_e = 0$ on $\mathcal{E}_h^\circ$ and $[\![u]\!]_e = g$ on $\mathcal{E}_h^b$. Subtracting the above equation from (4.2) yields (4.14). □

Theorem 4.1. Assume that Γ_b and Γ_i are of class C^{m+2}, that $\mathcal{T}_h$ is quasi-uniform with $h \leq h_0$, and that $\sigma_0 \geq \sigma_*$. If $u \in \mathcal{H}^{m+1}(\Omega)$ solves (1.3)–(1.5) and $u_h \in S_h^m(\mathcal{T}_h)$ is the solution of (4.2), then

$$\| u - u_h \|_{h,\beta} \leq C h^m \| u \|_{\mathcal{H}^{m+1}(\Omega)}. \tag{4.15}$$

Proof. For $v_h \in S_h^m(\mathcal{T}_h)$, set $\xi_h = v_h - u_h$. Coercivity, Galerkin orthogonality (4.14), and (4.12) give

$$\frac{1}{2} \| \xi_h \|_{h,\beta}^2 \leq a_h(\xi_h, \xi_h) = a_h(v_h - u, \xi_h) \leq |a_h(v_h - u, \xi_h)| \leq C |||u - v_h|||_{h,\beta} \| \xi_h \|_{h,\beta}.$$

It follows that $\| \xi_h \|_{h,\beta} \leq C |||u - v_h|||_{h,\beta}$. The triangle inequality and $\| u - v_h \|_{h,\beta} \leq |||u - v_h|||_{h,\beta}$ imply

$$\| u - u_h \|_{h,\beta} \leq C |||u - v_h|||_{h,\beta}.$$

Taking $v_h = \Pi_h u$ and applying (4.7) with $r = m + 1$, we obtain (4.15). □

For the L^2-error estimate, we consider the auxiliary problem: given $\psi \in L^2(\Omega)$, find $z \in H_0^1(\Omega)$ such that

$$\begin{aligned} -\nabla \cdot (\beta \nabla z) &= \psi \quad \text{in } \Omega^- \cup \Omega^+, \\ z &= 0 \quad \text{on } \Gamma_b, \\ [\![z]\!]_{\Gamma_i} = 0, \quad [\![\beta \partial_{\mathbf{n}} z]\!]_{\Gamma_i} &= 0 \quad \text{on } \Gamma_i. \end{aligned} \tag{4.16}$$

We assume that, for every $\psi \in L^2(\Omega)$, the auxiliary solution belongs to $\mathcal{H}^2(\Omega)$ and satisfies

$$\| z \|_{\mathcal{H}^2(\Omega)} \leq C_{\mathrm{reg}} \| \psi \|_{0,\Omega}. \tag{4.17}$$

Theorem 4.2. Under the assumptions of Theorem 4.1 and the adjoint regularity estimate (4.17), we have the following error estimate:

$$\|u-u_h\|_{0,\Omega} \le Ch^{m+1}\,\|u\|_{\mathscr{H}^{m+1}(\Omega)}\,.$$

Proof. Let $e_h = u-u_h$, and let z solve (4.16) with $\psi = e_h$. Since z satisfies the interface transmission conditions, the elementwise integration-by-parts argument used in Lemma 4.5 gives the adjoint consistency relation

$$a_h(w,z) = (w,e_h)_\Omega, \qquad w \in H^s(\mathscr{T}_h), \quad s > 3/2.$$

Hence, by Galerkin orthogonality,

$$\|e_h\|_{0,\Omega}^2 = a_h(e_h,z) = a_h(e_h, z-\Pi_h z).$$

A standard quasi-optimality argument based on coercivity, one-sided boundedness, and (4.10) yields

$$|||e_h|||_{h,\beta} \le C|||u-\Pi_h u|||_{h,\beta}.$$

Therefore, using (4.11), the primal and dual approximation estimates, and (4.17), we obtain

$$\begin{aligned}\|e_h\|_{0,\Omega}^2 &\le C|||u-\Pi_h u|||_{h,\beta}|||z-\Pi_h z|||_{h,\beta}\\ &\le Ch^{m+1}\,\|u\|_{\mathscr{H}^{m+1}(\Omega)}\,\|z\|_{\mathscr{H}^2(\Omega)}\\ &\le Ch^{m+1}\,\|u\|_{\mathscr{H}^{m+1}(\Omega)}\,\|e_h\|_{0,\Omega}\,.\end{aligned}$$

The desired estimate follows. □

4.3. **GC-FE approximation on a curved domain.** Although developed above for interface problems, GC-FE spaces also provide a geometry-exact alternative to classical isoparametric finite elements for higher-degree approximations on curved domains. Instead of replacing the curved boundary by a polynomial surrogate, the GC-FE construction retains the prescribed physical boundary as the curved edges of boundary elements and builds the local finite element spaces in the associated Frenet coordinates.

As an illustration, we apply the SIPDG-GC-FE method to the boundary value problem described by (1.1) and (1.2). The following corollary shows that the method attains optimal-order error estimates in the energy and L^2 norms without introducing a geometric approximation of Γ_b.

Corollary 4.1. Assume that Γ_b is of class C^{m+2}, that $\mathscr{T}_h$ is quasi-uniform with $h \le h_0$, and that $\sigma_0 \ge \sigma_*$. Let $u \in H^{m+1}(\Omega)$ solve (1.1) and (1.2), and, with $\Gamma_i = \emptyset$, let $u_h \in S_h^m(\mathscr{T}_h)$ solve (4.2). Then

$$\|u-u_h\|_{h,\beta} \le Ch^m\,\|u\|_{m+1,\Omega}\,.$$

If, in addition, the corresponding homogeneous-Dirichlet dual solution satisfies

$$\|z\|_{2,\Omega} \le C_{\mathrm{reg}}\,\|\psi\|_{0,\Omega}\,,$$

then

$$\|u-u_h\|_{0,\Omega} \le Ch^{m+1}\,\|u\|_{m+1,\Omega}\,.$$

Proof. The arguments of Theorems 4.1 and 4.2 apply with the corresponding one-domain spaces and norms. For the required approximation estimates, use the elementwise projection Π_h from (3.13). On $K \in \mathcal{T}_h^c$, use the curved-element projection associated with the physical-side fictitious element $K_F^{s_K} \subset \overline{\Omega}$; on $K \in \mathcal{T}_h^r$, use the standard $L^2(K)$-projection onto $\mathbb{P}_m(K)$. □

Remark 3. The corollary demonstrates that GC-FE spaces offer an alternative to isoparametric finite elements for higher-degree discretizations on curved domains. In a conventional isoparametric method, the physical boundary is generally replaced by a polynomial approximation, and the resulting geometric consistency error must be included in the analysis. In contrast, the GC-FE method retains the true boundary and its normal field through the Frenet representation. Consequently, the variational formulation is posed directly on the physical domain, thereby avoiding the geometric variational crime caused by boundary approximation. Moreover, boundary traces, normal fluxes, and edge integrals can be evaluated directly on the prescribed curved boundary.

5. Numerical Experiments

In this section, we present numerical experiments to assess the computational performance of GC-FE spaces within the SIPDG framework. We first examine the conditioning of the local mass matrices and compare the two basis-reconstruction approaches, RA1 and RA2. We then verify the predicted convergence rates for fitted interface and curved-boundary problems, compare GC-FE with nodal isoparametric finite elements, and demonstrate the unified GC-FE-GC-IFE method on meshes fitted to the outer boundary but unfitted to the internal interface.

5.1. **Choice of a well-conditioned basis for GC-FE computations.** We compare the condition numbers of the quadrature-based local mass matrices generated from the original GC-FE basis and the bases produced by RA1 and RA2. Specifically, for each $K \in \mathcal{T}_h^c$, we consider the three local bases $\boldsymbol{\phi}_K, \quad \widetilde{\boldsymbol{\phi}}_K^{(1)}, \quad \widetilde{\boldsymbol{\phi}}_K^{(2)}$ introduced in Subsection 3.2, and their corresponding local matrices:

$$\mathsf{M}_{q,K}(\boldsymbol{\phi}_K), \quad \mathsf{M}_{q,K}(\widetilde{\boldsymbol{\phi}}_K^{(1)}), \quad \mathsf{M}_{q,K}(\widetilde{\boldsymbol{\phi}}_K^{(2)}).$$

Table 1 reports the maximum 2-norm condition number over all curved elements of a representative mesh. The condition number for the original basis grows rapidly with the polynomial degree m. Both reconstructions substantially improve the conditioning, but the condition number of the mass matrix $\mathsf{M}_{q,K}(\widetilde{\boldsymbol{\phi}}_K^{(1)})$ begins to deteriorate at high degrees. By contrast, the condition number of the mass matrix $\mathsf{M}_{q,K}(\widetilde{\boldsymbol{\phi}}_K^{(2)})$ remains around 1 throughout the tested range. We therefore use the basis $\widetilde{\boldsymbol{\phi}}_K^{(2)}$ produced by RA2 on every curved GC-FE element in the numerical examples below.

5.2. **Accuracy of the SIPDG method for interface problems.** This example demonstrates the convergence behavior of the SIPDG-GC-FE method applied to an interface problem using interface-fitted meshes.

In the implementation of the SIPDG-GC-FE method, the finite element functions on straight-sided triangular elements are the standard ones such as those described in [21]. The precursor triangulations $\overline{\mathcal{T}}_h$ are generated using the MATLAB PDE Toolbox. We let $h = \max\{\mathrm{diam}(\overline{K}) : \overline{K} \in \overline{\mathcal{T}}_h\}$ denote the maximum element diameter of $\overline{\mathcal{T}}_h$.

TABLE 1. Maximum local mass-matrix condition numbers for the three GC-FE bases.

m	$\max_{K\in\mathcal{T}_h^c}\{\mathrm{cond}_2(\mathsf{M}_{q,K}(\boldsymbol{\phi}_K))\}$	$\max_{K\in\mathcal{T}_h^c}\left\{\mathrm{cond}_2(\mathsf{M}_{q,K}(\widetilde{\boldsymbol{\phi}}_K^{(1)}))\right\}$	$\max_{K\in\mathcal{T}_h^c}\left\{\mathrm{cond}_2(\mathsf{M}_{q,K}(\widetilde{\boldsymbol{\phi}}_K^{(2)}))\right\}$
1	2.8640×10^{1}	1.0000	1.0000
2	6.1557×10^{2}	1.0000	1.0000
3	1.3111×10^{4}	1.0000	1.0000
4	2.5122×10^{5}	1.0000	1.0000
5	1.2875×10^{7}	1.0000	1.0000
6	4.5506×10^{8}	1.0000	1.0000
7	1.7634×10^{10}	1.0000	1.0000
8	5.8544×10^{11}	1.0000	1.0000
9	2.2942×10^{13}	1.0010	1.0000
10	7.7187×10^{14}	1.6941	1.0000
11	4.7919×10^{16}	55.330	1.0000
12	5.6628×10^{18}	795.12	1.0000

The test interface problem is posed on $\Omega=\{(x,y): x^2/1.8^2+y^2/1.6^2<1\}$, which is an elliptical domain, and we let $\Gamma_b=\partial\Omega$. In polar coordinates (r,ϑ), define

$$\varphi_1(r,\vartheta)=r^5\big(1+0.5\sin(6\vartheta)\big)^2-\frac{\pi}{3}.$$

We then define the interface curve as the zero level set $\Gamma_i=\{\varphi_1=0\}$, which is a six-lobed flower-shaped curve. Let $\Omega^-=\{(x,y)\in\Omega:\varphi_1<0\}$ and $\Omega^+=\Omega\setminus\overline{\Omega^-}$, and let the piecewise constant coefficient β satisfy $\beta|_{\Omega^\pm}=\beta^\pm>0$; see the left panel of Figure 3 for illustrations of Ω,Γ_b,Γ_i and the mesh. We then choose f and g in the interface problem (1.3)-(1.5) such that the exact solution is

$$u_1(x,y)=\begin{cases}\dfrac{\cos(\varphi_1(x,y))}{\beta^-}, & (x,y)\in\Omega^-,\\[2mm] \dfrac{\cos(\varphi_1(x,y))}{\beta^+}+\dfrac{1}{\beta^-}-\dfrac{1}{\beta^+}, & (x,y)\in\Omega^+.\end{cases}\tag{5.1}$$

In all numerical experiments, we set the penalty parameter $\sigma_0=3$.

5.2.1. *Convergence of the SIPDG-GC-FE method.* Table 2 reports the convergence rates of the SIPDG-GC-FE method when used to solve the interface problem on a sequence of fitted meshes and the following set of diffusion coefficients representing some typical jump contrasts:

$$(\beta^-,\beta^+)\in\{(1000,1),\ (10,1),\ (1,10),\ (1,1000)\}.$$

Figure 4 presents the L^2 and broken H^1-seminorm error data for $m=1,2,3,4$ with $(\beta^-,\beta^+)=(1,1000)$. The observed L^2 and broken H^1-seminorm errors exhibit convergence behavior reported in Table 2, which is consistent with the respective $O(h^{m+1})$ and $O(h^m)$ estimates in Theorems 4.1–4.2.

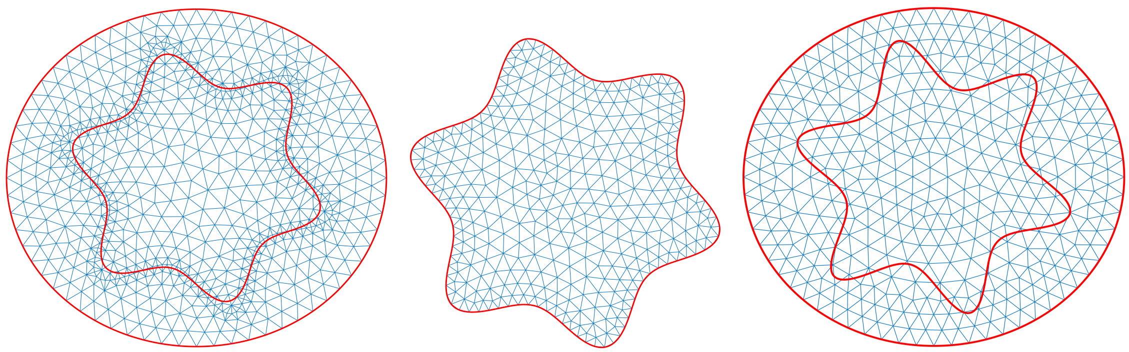

FIGURE 3. From left: a mesh fitted to the outer boundary and internal interface used in Subsection 5.2; a boundary-fitted mesh for the flower-shaped domain used in Subsection 5.3; and a boundary-fitted, interface-unfitted mesh used in Subsection 5.4.

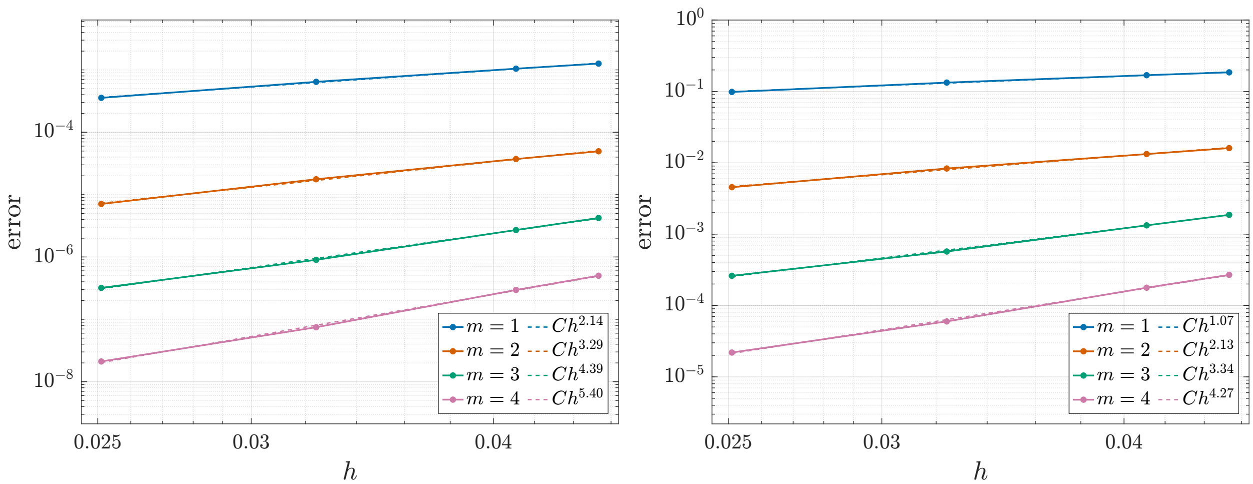

(A) L^2-norm error.

(B) Broken H^1-seminorm error.

FIGURE 4. Convergence of SIPDG-GC-FE solutions with $(\beta^-, \beta^+) = (1, 1000)$ and $1 \le m \le 4$.

TABLE 2. Convergence rates for SIPDG-GC-FE solutions with various coefficient contrasts.

m	$(\beta^-,\beta^+) = (1000,1)$		$(\beta^-,\beta^+) = (10,1)$		$(\beta^-,\beta^+) = (1,10)$		$(\beta^-,\beta^+) = (1,1000)$	
	L^2	broken H^1	L^2	broken H^1	L^2	broken H^1	L^2	broken H^1
1	1.91	1.06	1.91	1.06	1.91	1.06	2.14	1.07
2	3.28	2.08	3.28	2.08	3.28	2.08	3.29	2.13
3	4.39	3.35	4.39	3.35	4.39	3.35	4.39	3.34
4	5.40	4.27	5.40	4.27	5.40	4.27	5.40	4.27

5.2.2. *Local accuracy using GC-FE spaces.* We now compare the SIPDG-GC-FE method with a standard nodal isoparametric finite element DG method (SIPDG-ISO-FE) [21]. Both methods are applied to the interface problem considered above using the same straight-sided precursor meshes, polynomial degrees, SIPDG formulation, and penalty parameter $\sigma_0 = 3$, with $(\beta^-, \beta^+) = (1, 1000)$. The comparison therefore isolates the effect of their different treatments of curved geometry: GC-FE conforms exactly to the prescribed outer boundary and interface, whereas ISO-FE represents these curves by isoparametric polynomial approximations.

Figure 5 reports the errors in the L^2 norm and broken H^1 seminorm. The corresponding curves nearly coincide, indicating that the SIPDG-GC-FE and SIPDG-ISO-FE methods achieve comparable global accuracy.

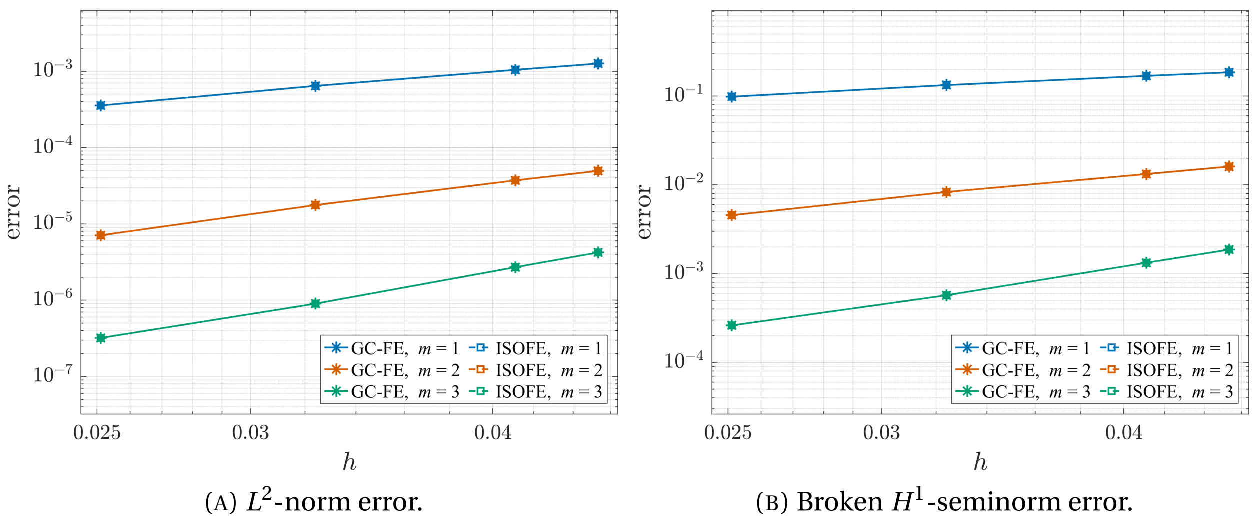

FIGURE 5. Global errors of SIPDG-GC-FE and SIPDG-ISO-FE on fitted meshes of the elliptical domain Ω, with $(\beta^-, \beta^+) = (1, 1000)$ and $m = 1, 2, 3$.

We next compare the trace errors on the true interface. Specifically, at each interface sample point, we evaluate $|u - \{\!\{u_h\}\!\}|$, where $\{\!\{u_h\}\!\}$ denotes the average of the two DG traces. On each prescribed interface segment, we use the same set of 40 sample points for both methods and record the maximum sampled error.

Figure 6 reports the resulting errors for $m = 1, 2$. Both methods use the same straight-sided precursor mesh with $h = 7.30 \times 10^{-2}$. For SIPDG-ISO-FE, the true-interface sample points generally do not lie on the approximate interface. The two traces at each sample point are therefore evaluated by extending the finite element functions from the two corresponding isoparametric elements.

For $m = 1$, SIPDG-GC-FE produces substantially smaller sampled errors than SIPDG-ISO-FE, which uses a piecewise linear approximation of the interface. For $m = 2$, the difference becomes smaller, but the SIPDG-GC-FE error remains lower in this test.

5.3. **Convergence of the SIPDG-GC-FE method on a curved domain.** This example demonstrates the use of the SIPDG-GC-FE method for a boundary value problem on a curved domain. In polar coordinates (r, ϑ), define $\phi_2(r, \vartheta) = r^4\big(1 + 0.3\sin(6\vartheta)\big)^2 - \pi/3$. We consider the boundary

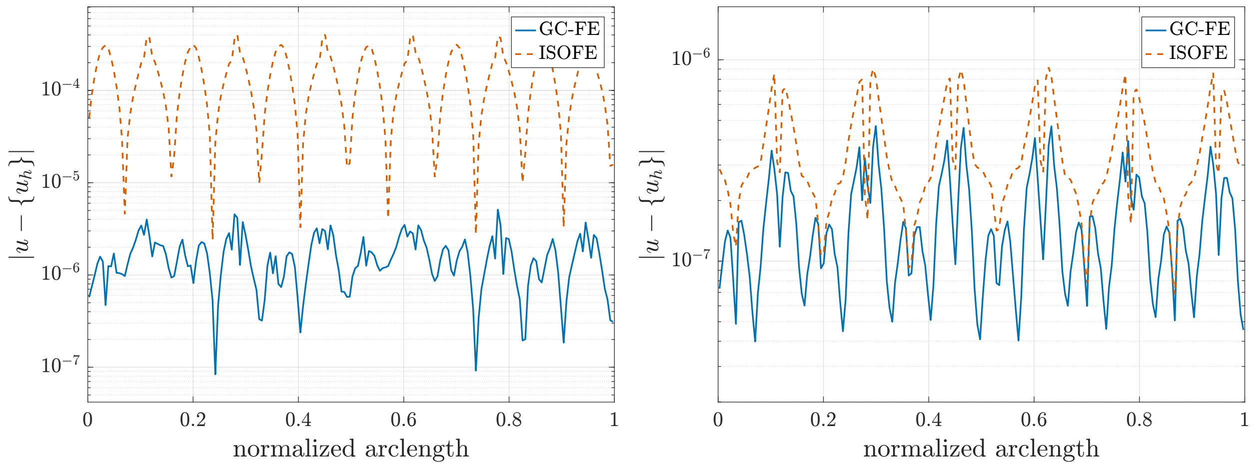

(A) $m = 1$. (B) $m = 2$.

FIGURE 6. Sampled pointwise errors $|u - \{\!\{u_h\}\!\}|$ along the true interface for SIPDG-GC-FE and SIPDG-ISO-FE with $(\beta^-, \beta^+) = (1, 1000)$ and $h = 7.30 \times 10^{-2}$.

value problem (1.1)–(1.2) on $\Omega = \{\phi_2 < 0\}$, $\Gamma_b = \partial\Omega = \{\phi_2 = 0\}$. The domain and a corresponding mesh are shown in the middle panel of Figure 3. The diffusion coefficient is chosen as $\beta(x, y) = 1 + x^2 + y^2$, and the source term f and boundary data g are chosen so that the exact solution is $u(x, y) = \cos(\pi x)\sin(\pi y)$.

Figure 7 presents the L^2-norm and broken H^1-seminorm errors of the SIPDG-GC-FE solutions computed in $S_h^m(\mathcal{T}_h)$ on a sequence of five successively refined meshes. The observed convergence rates corroborate the $O(h^{m+1})$ and $O(h^m)$ error estimates, respectively, established in Corollary 4.1.

Together with Corollary 4.1, these numerical results support the use of the GC-FE method as a geometry-exact alternative to other higher-degree finite element methods for solving boundary value problems on curved domains.

5.4. **A unified high-order treatment of curved boundaries and unfitted interfaces: GC-FE-GC-IFE method.** This example demonstrates how GC-FE spaces can be coupled with geometry-conforming immersed finite element (GC-IFE) spaces to solve the interface problem (1.3)–(1.5) on a curved domain using an interface-unfitted mesh. As described in Section 2, such a mesh can be decomposed as

$$\mathcal{T}_h = \mathcal{T}_h^i \cup \mathcal{T}_h^c \cup \mathcal{T}_h^r, \qquad \mathcal{T}_h^i \neq \emptyset.$$

We define the following hybrid GC-FE-GC-IFE space:

$$\widetilde{S}_h^m(\mathcal{T}_h) = \left\{ v_h \in L^2(\Omega) : v_h|_K \in \begin{cases} S_h^m(K), & K \in \mathcal{T}_h^c, \\ S_{h,\mathrm{IFE}}^m(K), & K \in \mathcal{T}_h^i, \\ \mathbb{P}_m(K), & K \in \mathcal{T}_h^r \end{cases} \text{for every } K \in \mathcal{T}_h \right\}.$$

Here, $S_{h,\mathrm{IFE}}^m(K)$ denotes the degree-m local GC-IFE space developed in [29]. The unified SIPDG-GC-FE-GC-IFE method is obtained from the SIPDG formulation (4.2) by using $\widetilde{S}_h^m(\mathcal{T}_h)$ as both the trial and test space.

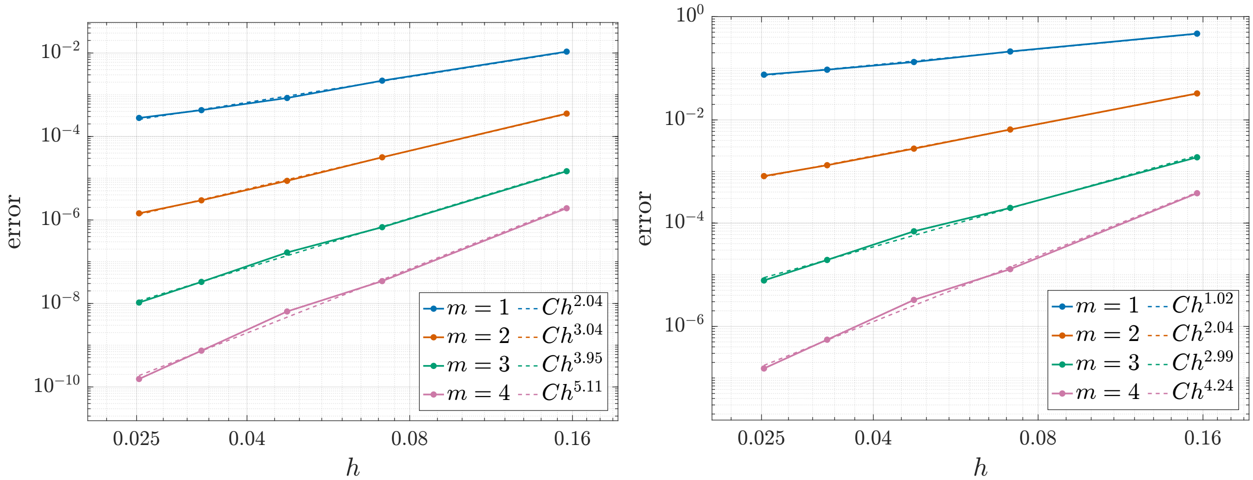

(A) L^2-norm error.

(B) Broken H^1-seminorm error.

FIGURE 7. Convergence of the SIPDG-GC-FE method for the variable-coefficient problem on the six-lobed flower-shaped domain: (A) L^2-norm error; (B) broken H^1-seminorm error.

Table 3 reports the observed convergence rates for the interface problem specified in Section 5.2, computed on a sequence of interface-unfitted meshes for the diffusion-coefficient pairs

$$(\beta^-, \beta^+) \in \{(1000, 1),\ (10, 1),\ (1, 10),\ (1, 1000)\}.$$

These pairs represent moderate and large coefficient jumps in both directions. The domain Ω, outer boundary Γ_b, interface Γ_i, and a representative unfitted mesh are shown in the right panel of Figure 3. Figure 8 presents the L^2-norm and broken H^1-seminorm errors versus h for $m = 1, \ldots, 4$, with $(\beta^-, \beta^+) = (1, 1000)$.

The observed rates are consistent with the optimal $O(h^{m+1})$ and $O(h^m)$ convergence orders in the L^2 norm and broken H^1 seminorm, respectively, for all tested polynomial degrees and coefficient pairs. These results indicate that the unified SIPDG-GC-FE-GC-IFE method provides a viable high-order approach to interface problems on curved domains using meshes independent of the interface.

TABLE 3. Convergence rates obtained by linear regression for the unified SIPDG-GC-FE-GC-IFE method.

m	$(\beta^-, \beta^+) = (1000, 1)$		$(\beta^-, \beta^+) = (10, 1)$		$(\beta^-, \beta^+) = (1, 10)$		$(\beta^-, \beta^+) = (1, 1000)$	
	L^2	broken H^1	L^2	broken H^1	L^2	broken H^1	L^2	broken H^1
1	1.85	1.01	1.85	1.01	1.85	1.01	2.08	1.01
2	3.09	2.00	3.09	2.00	3.09	2.00	3.05	1.98
3	3.96	3.04	3.96	3.04	3.96	3.04	3.96	3.04
4	4.91	3.95	4.91	3.95	4.91	3.95	4.84	3.88

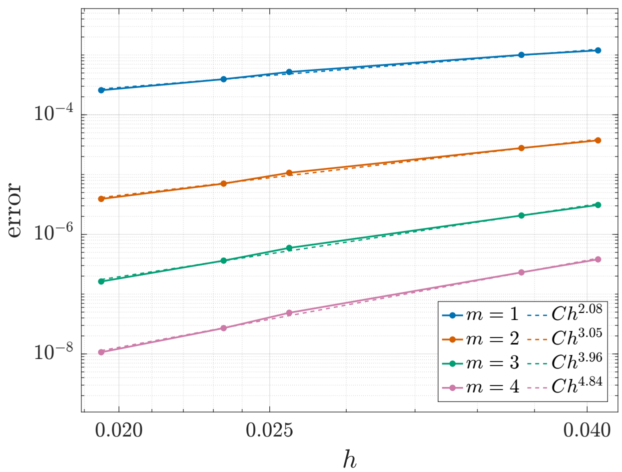

(A) L^2-norm error.

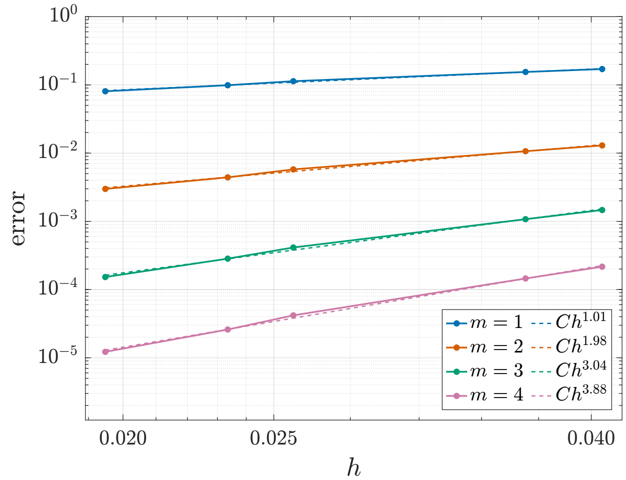

(B) Broken H^1-seminorm error.

FIGURE 8. Errors of the unified SIPDG-GC-FE-GC-IFE method with a fitted outer boundary and an unfitted internal interface, for $(\beta^-, \beta^+) = (1, 1000)$ and $m = 1, 2, 3, 4$.

6. CONCLUSIONS

We developed an arbitrary-degree GC-FE framework for curved-boundary and interface problems. By constructing polynomial spaces in Frenet coordinates, the method retains the exact physical curves while producing generally nonpolynomial shape functions in Cartesian coordinates. We established optimal approximation, inverse, and trace estimates and proved well-posedness and optimal bounds in the energy and L^2 norms for the SIPDG discretization without requiring separate geometric consistency estimates. The numerical results confirmed the predicted rates, showed that GC-FE is competitive with the nodal isoparametric method, and demonstrated its effective coupling with GC-IFE spaces on interface-unfitted meshes. Thus, the framework provides a unified, geometry-conforming, high-order treatment of curved boundaries and fitted or unfitted interfaces.

REFERENCES

1. Marco Abate and Francesca Tovena, *Curves and surfaces*, Springer Science & Business Media, 2012.
2. E. Abbena, S. Salamon, and A. Gray, *Modern differential geometry of curves and surfaces with Mathematica*, 3rd ed., Chapman and Hall/CRC, 2006.
3. Slimane Adjerid, Ruchi Guo, and Tao Lin, *High degree immersed finite element spaces by a least squares method*, Int. J. Numer. Anal. Model. **14** (2017), no. 4-5, 604–626.
4. Slimane Adjerid, Tao Lin, and Haroun Meghaichi, *A high order geometry conforming immersed finite element for elliptic interface problems*, Comput. Methods Appl. Mech. Engrg. **420** (2024), 116703.
5. ______, *The Frenet immersed finite element method for elliptic interface problems: an error analysis*, Comput. Methods Appl. Mech. Engrg. **438** (2025), 117829.
6. Slimane Adjerid, Tao Lin, and Haroun Meghaichi, *Construction of basis functions for the geometry conforming immersed finite element method*, Numer. Algorithms (2026), no. accepted, arXiv:2510.12018.
7. Slimane Adjerid and Kihyo Moon, *An immersed discontinuous Galerkin method for acoustic wave propagation in inhomogeneous media*, SIAM J. Sci. Comput. **41** (2019), no. 1, A139–A162.

8. Yuan Chen and Xu Zhang, *A P_2-P_1 partially penalized immersed finite element method for Stokes interface problems*, Int. J. Numer. Anal. Model. **18** (2021), no. 1, 120–141.
9. ______, *An immersed C^0 interior penalty finite element method for biharmonic interface problems*, J. Sci. Comput. **108** (2026), Paper No. 38.
10. P. G. Ciarlet and P.-A. Raviart, *The combined effect of curved boundaries and numerical integration in isoparametric finite element methods*, The mathematical foundations of the finite element method with applications to partial differential equations, Academic Press, 1972, pp. 409–474.
11. ______, *Interpolation theory over curved elements, with applications to finite element methods*, Comput. Methods Appl. Mech. Engrg. **1** (1972), no. 2, 217–249.
12. Philippe G. Ciarlet, *The finite element method for elliptic problems*, North-Holland Publishing Co., Amsterdam-New York-Oxford, 1978, Studies in Mathematics and its Applications, Vol. 4.
13. W. J. Gordon and C. A. Hall, *Transfinite element methods: Blending-function interpolation over arbitrary curved element domains*, Numer. Math. **21** (1973), 109–129.
14. William J. Gordon and Charles A. Hall, *Construction of higher order curved elements with large aspect ratios, using coordinate transformations*, Int. J. Numer. Methods Eng. **7** (1973), no. 4, 461–477.
15. Ruchi Guo and Tao Lin, *A higher degree immersed finite element method based on a Cauchy extension for elliptic interface problems*, SIAM J. Numer. Anal. **57** (2019), no. 4, 1545–1573.
16. ______, *An immersed finite element method for elliptic interface problems in three dimensions*, J. Comput. Phys. **414** (2020), no. 1, 109478.
17. Ruchi Guo, Tao Lin, and Yanping Lin, *Error estimates for a partially penalized immersed finite element method for elasticity interface problems*, ESAIM Math. Model. Numer. Anal. **54** (2020), no. 1, 1–24.
18. Ruchi Guo and Xu Zhang, *Solving three-dimensional interface problems with immersed finite elements: A-priori error analysis*, J. Comput. Phys. **441** (2021), 110445.
19. Xiaoming He, Tao Lin, and Yanping Lin, *Approximation capability of a bilinear immersed finite element space*, Numer. Methods Partial Differential Equations **24** (2008), no. 5, 1265–1300.
20. Xiaoming He, Tao Lin, Yanping Lin, and Xu Zhang, *Immersed finite element methods for parabolic equations with moving interface*, Numer. Methods Partial Differential Equations **29** (2013), no. 2, 619–646.
21. Jan S. Hesthaven and Tim Warburton, *Nodal discontinuous Galerkin methods*, Texts in Applied Mathematics, vol. 54, Springer, New York, 2008, Algorithms, analysis, and applications.
22. Haifeng Ji, Zhifeng Weng, and Qian Zhang, *An augmented immersed finite element method for variable coefficient elliptic interface problems in two and three dimensions*, J. Comput. Phys. **418** (2020), 109631.
23. M. Lenoir, *Optimal isoparametric finite elements and error estimates for domains involving curved boundaries*, SIAM J. Numer. Anal. **23** (1986), no. 3, 562–580.
24. Jingzhi Li, Jens M. Melenk, Barbara Wohlmuth, and Jun Zou, *Optimal a priori estimates for higher order finite elements for elliptic interface problems*, Appl. Numer. Math. **60** (2010), no. 1–2, 19–37.
25. Zhilin Li, *The immersed interface method using a finite element formulation*, Appl. Numer. Math. **27** (1998), no. 3, 253–267.
26. Zhilin Li, Tao Lin, and Xiaohui Wu, *New Cartesian grid methods for interface problems using the finite element formulation*, Numer. Math. **96** (2003), no. 1, 61–98.
27. Tao Lin, Yanping Lin, and Xu Zhang, *Partially penalized immersed finite element methods for elliptic interface problems*, SIAM J. Numer. Anal. **53** (2015), no. 2, 1121–1144.
28. Tao Lin, Dongwoo Sheen, and Xu Zhang, *A locking-free immersed finite element method for planar elasticity interface problems*, J. Comput. Phys. **247** (2013), 228–247. MR 3066172
29. Yuanhui Lin, Xu Zhang, and Tao Lin, *Frenet immersed finite element spaces on triangular meshes*, Int. J. Numer. Anal. Model. (2026), in press.
30. Barrett O'Neill, *Elementary differential geometry*, second ed., Academic Press, 2006.
31. Beatrice Rivière, *Discontinuous Galerkin methods for solving elliptic and parabolic equations*, Frontiers in Applied Mathematics, vol. FR35, SIAM, Philadelphia, 2008.
32. Gilbert Strang and George J. Fix, *An analysis of the finite element method*, Prentice-Hall Series in Automatic Computation, Prentice-Hall, Inc., Englewood Cliffs, NJ, 1973. MR 443377

33. Hua Wang, Jinru Chen, Pengtao Sun, and Fangfang Qin, *A conforming enriched finite element method for elliptic interface problems*, Applied Numerical Mathematics **127** (2018), 1–17.

SCHOOL OF MATHEMATICS, SICHUAN UNIVERSITY, CHENGDU, SICHUAN 610065, CHINA.
Email address: linyuanhui001@stu.scu.edu.cn

DEPARTMENT OF MATHEMATICS, VIRGINIA TECH, BLACKSBURG, VA 24060, USA.
Email address: tlin@vt.edu

DEPARTMENT OF MATHEMATICS, OKLAHOMA STATE UNIVERSITY, STILLWATER, OK 74078, USA.
Email address: xzhang@okstate.edu

SCHOOL OF MATHEMATICS, SICHUAN UNIVERSITY, CHENGDU, SICHUAN 610065, CHINA.
Email address: fmf@scu.edu.cn